國 立 交 通 大 學
運 輸 科 技 與 管 理 學 系

博 士 論 文

雷達車輛偵測及衝擊波技術應用於緊鄰路口號誌控制之研究

Radar Vehicle Detection and Shockwave Techniques for Signal Control of Closely Spaced Intersections

研究生： 曾明德

指導教授：卓訓榮 教授

中華民國一〇一年七月

雷達車輛偵測及衝擊波技術應用於緊鄰路口號誌控制之研究

Radar Vehicle Detection and Shockwave Techniques for Signal Control of Closely Spaced Intersections

研 究 生：曾明德　　　　　　　　　　　　Student：Ming-Te Tseng

指導教授：卓訓榮　　　　　　　　　　　　Advisor：Hsun-Jung Cho

國 立 交 通 大 學

運輸科技與管理學系

博 士 論 文

A Dissertation

Submitted to Department of Transportation Technology and Management

College of Management

National Chiao Tung University

in Partial Fulfillment of the Requirements

for the Degree of

Doctor of Philosophy

in

Transportation Technology and Management

July 2012

Hsinchu, Taiwan, Republic of China

中華民國一〇一年七月

雷達車輛偵測及衝擊波技術應用於緊鄰路口號誌控制之研究

學生：曾明德　　　　　　　　　　　　　　指導教授：卓訓榮

國立交通大學運輸科技與管理學系 博士班

摘　要

　　在尖峰時刻，市區或高速公路匝道附近，常常會有數個緊鄰路口的交通擁塞問題，其中號誌控制不當也常是擁堵主因。而在作智慧型的號誌控制中，車輛偵測器的車流偵測能力更是關鍵因子。因此本研究從車輛偵測器開始研究，除了偵測傳統流量、速度之外，並偵測十字路口衝擊波，並應用該衝擊波技術作緊鄰路口的號誌控制。

　　本研究首先針對雷達車輛偵測器，提出車種、車速的演算法。該演算法以最佳辨識演算法為基礎，結合影像處理來學習，使用支持向量機 (Support Vector Machine)來辨識車種、支持向量迴歸 (Support Vector Regression)來估計車長及分辨車種。以市區道路蒐集到的真實資料驗證，並比較 K-mean 及線性判別分析法 (Linear Discriminant Analysis)後，証實支持向量機及支持向量迴歸可成功精確地辨識機車、小車、大車及超大車等多種車長及推估其速度。

　　接著，本研究利用前述雷達偵測器的偵測結果，提出新的三個交通參數:空車、有車及停車，並利用此三參數結合車流理論導出路口衝擊波的偵測方法，而且也在模擬環境成功驗證其可行性及精確程度。

　　最後本研究，提出一個以傳統觸動控制為基礎的臨界路徑控制方法，該方法以關鍵行車路徑來設計時相、依車流回堵情形動態調整路徑時相最大綠燈時間並在萬一車流在綠燈停止不動時，切換時相以避免路口容量損失。該方法中，並以衝擊波理論為基礎推估各臨界路徑上需求綠燈時間，進而提出最佳化模式，求解各路徑最佳均衡綠燈時間。另外,也在一個實際的緊鄰路口組成的群組路口，模擬運作情形，比起傳統觸動模式有顯著改善。

Radar Vehicle Detection and Shockwave Techniques for Signal Control of Closely Spaced Intersections

Student: Ming-Te Tseng   Advisors: Hsun-Jung Cho

Department of Transportation Technology and Management

National Chiao Tung University

ABSTRACT

A complementary metal-oxide semiconductor based radar with sensitivity time control antenna is successfully implemented for advanced traffic signal processing. The collected signals from the radar system are processed with developed optimization algorithms for vehicle-type classification and speed determination. In course of optimization, a video recognition module is further adopted as a supervisor of support vector machine and support vector regression. In the meanwhile, skew training data set and numerous classification scenarios are used to test the classifiers. Finally, the results are analyzed and compared.

Beside, this investigation provides two traffic flow detection methods for oversaturated signalized intersection. The first method detects intersection shockwaves by innovative traffic parameters involving stopped duration, moving duration, and empty duration. The second method provides upstream arrival rate and speed by shockwaves, signal timing, and traffic flow model. This research has a contribution to the detection of shockwaves and upstream traffic parameters under over-saturated condition which traditional detectors cannot provide.

Finally, a novel actuated critical path control model for designing signal timings on closely spaced intersections is presented in this study. Shockwaves are utilized to dynamically adjust maximal green time for each critical path with unstable traffic demands. Combined with path-based progression, this methodology suggests a novel way to deal with closely spaced intersections. A real network had been exemplified with micro-simulation to illustrate the effectiveness of the proposed method. The numerical example demonstrates a satisfying result compare to ordinary full-actuated scheme.

誌　　謝

Table of Contents

LIST OF FIGURES

LIST OF TABLES

I. Introduction

1.1 Background

Accurate methods of collecting traffic information are essential in an intelligent transportation system (ITS). Traffic data has been gathered primarily via inductive loop detectors, pneumatic road tubes, and temporary manual counts. However, traffic detectors developed recently use video, sonic, ultrasonic, radar or infrared energy. These detectors are non-intrusive and mounted either overhead or to the side of traffic lanes. Considering the cost, radar and video sensors both have multi-lanes capability. A single detector of either of these types can detect up to eight or ten lanes. However, poor weather conditions, such as snow and heavy rain, can seriously impact video sensors. In contrast, radar sensors still function effectively in poor weather. Therefore, radar sensors are a good choice in ITS applications owing to their multi-lane coverage and resistance to weather impacts.

Numerous classifiers have been developed and tested for data cluster or pattern recognition, and these classifiers are categorized into two types: supervised and unsupervised. In supervised learning, the aim is to learn a mapping from the input to an output whose correct vehicle classes are provided by a supervisor. In unsupervised learning, there is no such supervisor and we only have input of data. K-mean cluster is a famous unsupervised classifier that has been used for numerous applications. Furthermore, support vector machine (SVM) and linear discriminated analysis (LDA) are two supervised classifiers. LDA was originally developed in 1936 by R.A. Fisher. SVMs have been used for isolated handwritten digit recognition, object recognition, speaker identification and face detection in images. To find the optimal classifier, this study tests these three classifiers under two constraints. Vehicle speed is estimated using

a virtual loop concept that requires vehicle and virtual loop length to make an estimate. Support vector regression (SVR) is used to predict vehicle length, while a video calibrating system is used to measure virtual loop length. A skew training data set and numerous classification scenarios are used to test the classifiers.

According to the Doppler Effect, the frequency of the radio wave will become higher than the original frequency when the object approaches the radar device, and the frequency of the radio wave will become lower than the original frequency when the object moves away from the radar device. Therefore, the frequency variations of the reflective signal is analyzed to acquire vehicle's speed; in other word, when a vehicle moves at a high enough speed to generate the Doppler Effect, the reflective radio wave from the vehicle will generate the Doppler shift. The Doppler frequency versus time variations of the reflective radio wave is recorded and the relative speed of the vehicle and the radar can be computed.

Real-time upstream traffic information is important because adaptive models must have them to predict future traffic flow and compute the signal timing. Under non-oversaturated situation, vehicle detectors can provide such real-time upstream information. However, vehicle detectors are not capable to provide upstream flow accurately under oversaturated traffic condition; vehicles often have a full stop at detection zone and the detected flow is not "arrival" but "departure". Hence, this research utilizes another robust oversaturated traffic parameter, shockwave. The shockwave detection methodology is also proposed to show its effectiveness.

To estimate shockwaves under oversaturated traffic situation, this research utilizes innovative traffic parameters, including stopped duration, moving duration, and empty duration; which depend only on the presence of vehicle and remain accurate even under oversaturated condition.

Closely spaced intersections are characterized as having short link distance between intersections; the physical spacing between the intersections is small. These intersections often become traffic bottleneck during peak hours due to its physical configuration. With inappropriate signal design and short links, traffic queues are likely to spill-back and cause an inefficient signal operation. The jammed traffic is generally derived from poor progression or unstable demands. Poor coordination of the signals leads to queue spill-back from one intersection that can seriously disrupt operation of the adjacent intersection. Furthermore, although several methods have been used to mitigate the congestion of closely spaced intersection, they seldom focused on the crooked traffics of the adjacent minor approaches. As the traffic demand on minor approaches grows, progression on those approaches should also be introduced. Despite the contribution of those researches, most of such models have not addressed such progression issue. Traffics in closely spaced intersections are treated as paths in this study. These paths would unfold hiding conflict points which would not easily be seen while considering flows on different approaches only. These conflict points often cause safety and efficiency issues, especially during oversaturated periods. Therefore, progressions in these closely spaced intersections have a multi-path nature rather than two-way progression on arterials.

1.2 Problem definition

The mixing of motorcycles and other traffic is hazardous in Asia. Currently, most radar detection algorithms classify vehicles into three or five categories, but generally exclude motorcycles from the classification system. How to detect motorcycles by radar sensor should be focused. Beside, speed estimation is not accurate for single transceiver Radar sensor, an accurate estimation method for vehicle speed needs to be developed.

Vehicle detectors are not capable to provide upstream flow accurately under oversaturated traffic condition; vehicles often have a full stop at detection zone and the detected flow is not "arrival" but "departure". The shockwave is a robust detectable parameter under oversaturated traffic condition and has been applied to traffic control for a long time. An accurate estimation method for shockwave needs to be developed.

Closely spaced intersections often become traffic bottleneck during peak hours due to its physical configuration. The jammed traffic is generally derived from poor progression or unstable demands. Therefore, phasing sequence design and dynamic green time adjustment need to be solved analytically.

1.3 Research objectives

The main objectives of this research effort can be summarized as follows:

To find a high recognition rate optimization algorithm for the vehicle-type classification and speed determination of radar detector.

To provide two upstream flow estimation methods for oversaturated signalized intersections; both methods are based on shockwaves of a signalized intersection. The first method calculates shockwaves by combining the new traffic parameters and traffic flow model. The second method makes use of the shockwaves derived from method one and provides upstream flow estimation.

To find a signal control method to mitigate the oversaturated traffic condition in closely spaced intersections.

1.4 Research contributions

This study illustrates a radar sensor classification scheme that classifies vehicles into four categories: motorcycles, small, medium and large vehicles. This research has

successfully combine two supervised learning algorithms to do vehicle classification and speed estimation: support vector machine and support vector regression.

The shockwave estimation method contributes 1) providing a general estimation method for five shockwaves in an intersection, 2) the model formulation takes dynamic signal timing into consideration, 3) the capability of predicting required green time to discharge traffic queue, and 4) introducing an upstream flow estimation method that capable to provide information beyond the detection zone of vehicle detectors.

The proposed signal control method which can: (1) improve signal operation by path-based progression instead of two-way progression, (2) introduce a novel phase change concept for full-actuated control to prevent capacity loss, and (3) modify existing full-actuated control to suit the closely spaced intersections and to dynamically adjust maximal green time according to unstable traffic demands.

1.5 Research layout

This dissertation is organized as follows. First, the introduction chapter gives an overview of the background, problem definition, research objectives, contributions and overview of this dissertation. Second, chapter 2 presents a literature review of related researches in the relevant areas. The literature review chapter concerns about topics, including: i) radar vehicle detection algorithms, ii) Shockwave detection and iii) signal control methods.

Radar vehicle detection algorithm, shockwaves detection model and optimal signal control algorithm for closely spaced intersections are proposed in chapter 3. In chapter 4, numerical examples with real data for radar vehicle detector are discussed; shockwaves and closely spaced intersections are simulated. The last chapter presents the conclusions and perspectives of this study.

II Literature Review

This chapter provides literature reviews relevant to the formulation and solution algorithm of radar vehicle detection, shockwave estimation and closely spaced signal control problem. The following sections are organized as (i) radar detection algorithms, (ii) shockwave detection algorithms, (iii) signal control methods

2.1 Radar vehicle detection
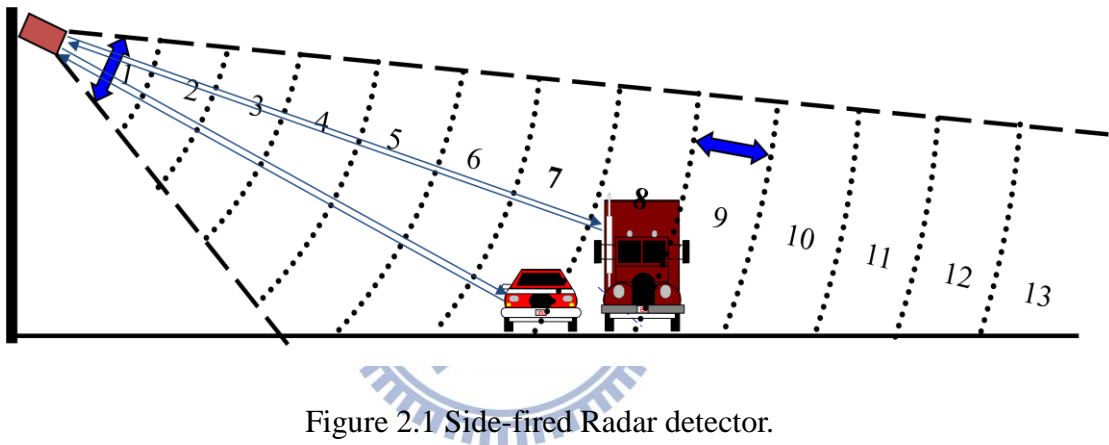
Figure 2.1 Side-fired Radar detector.
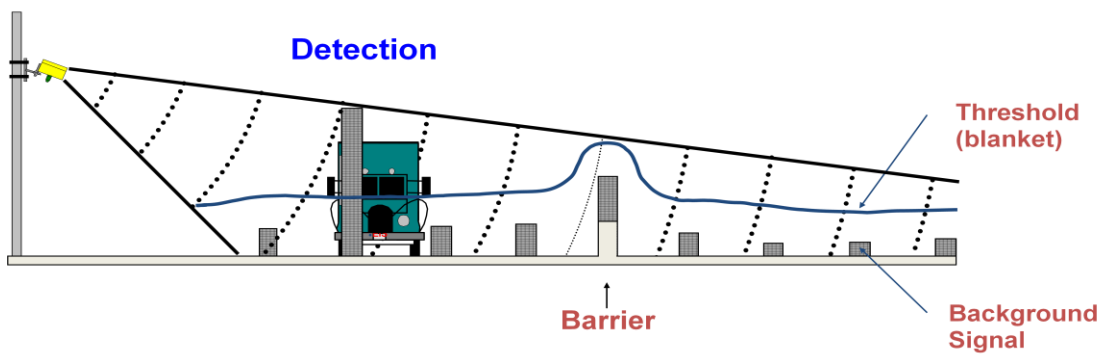
Figure 2.2 Radar signal power over road surface.

Microwave radar was developed for detecting objects. The word radar was derived from the function that it performs: Radio Detection and Ranging. The term microwave refers to the wavelength of the transmitted energy of 1GHz to 30 GHz. Microwave sensors designed for traffic data collection are limited to intervals near 10.525 or 24.0 GHz. Sensors with 10.525GHz have lower range resolution , bigger size and lower cost than sensors with 24Ghz.

Microwave sensors are generally mounted as side-fire configuration (as Figure 2.1). Side-fire mode is mounted on a roadside pole with its footprint aimed at right angle to the traffic lanes.   Side-fire mode can monitor up to 10 lanes for each sensor. The sensor receives the reflected signals from all surfaces within its beam − pavement, barriers, vehicles and trees. It maintains a background signal level from fixed objects in each range slices. Vehicles are detected when their reflected signal exceeds the background level of their range slice by a certain amount called threshold (see Figure 2.2).

The main types of microwave radar sensors are used in roadside are Frequency Modulated Continuous Wave (FMCW) radar [1, 2] in which the transmitted frequency is constantly changing with respect to time, as illustrated in Figure 2.3. The FMCW radar operates as a presence detector and can detect motionless vehicles.

The carrier frequency increases linearly with time. The ramp slope is given by $\Delta f/\Delta t$. The echo is received after the round trip time Tr = 2R/c where R is the distance to the target. The echo is mixed with a portion of the transmitted signal to produce an output beat frequency,

$$f_b = \frac{R}{\Delta R} \tag{2.1}$$

where $\Delta R = \frac{c}{2\Delta f}$ is range resolution.

A moving vehicle will superimpose a Doppler frequency shift on the beat frequency f_d. One portion of the beat frequency will be increased and the other portion will be decreased. For a target approaching the radar, the received signal frequency is increased (shifted up in the diagram) decreasing the up-sweep beat frequency and increasing the down-sweep beat frequency (see Figure 2.4)

$$f_b(up) = f_b - f_d, \tag{2.2}$$

$$f_b(dn) = f_b + f_d.$$

If we look at the Doppler frequency when a vehicle passes through the radar antenna beam, the Doppler shift of a reflected signal is proportional to the velocity of the vehicle and to the angle at which the signal is reflected. This relationship is described by the equation: $f_d = \frac{2v Sin\theta}{\lambda}$ (see Figure 2.5).

For small angle $Sin\,\theta = \theta$, hence

$$f_d = \frac{2v Sin\theta}{\lambda} = \frac{2v^2 t}{\lambda d} \tag{2.3}$$

Therefore, the Doppler shift changes linearly and pass through zero as the vehicle pass through the sensor's field of view [3](As Figure 2.5). The slope of this linear change is a function of the velocity of the target and the distance of the target's path from the sensor. The Doppler shift of reflected angle is measured multiple times as the vehicle passes through the field of view of side fire sensor. A linear fit is applied to the Doppler shift measurements and results in a slope m. The slop m is converted to a speed by

$$v = \sqrt[2]{md\lambda/2}. \tag{2.4}$$

Another vehicle speed estimating method is to use the virtual loop concept [4, 5, 6], which a detection zone of a radar is realized as an inductive loop on the ground.
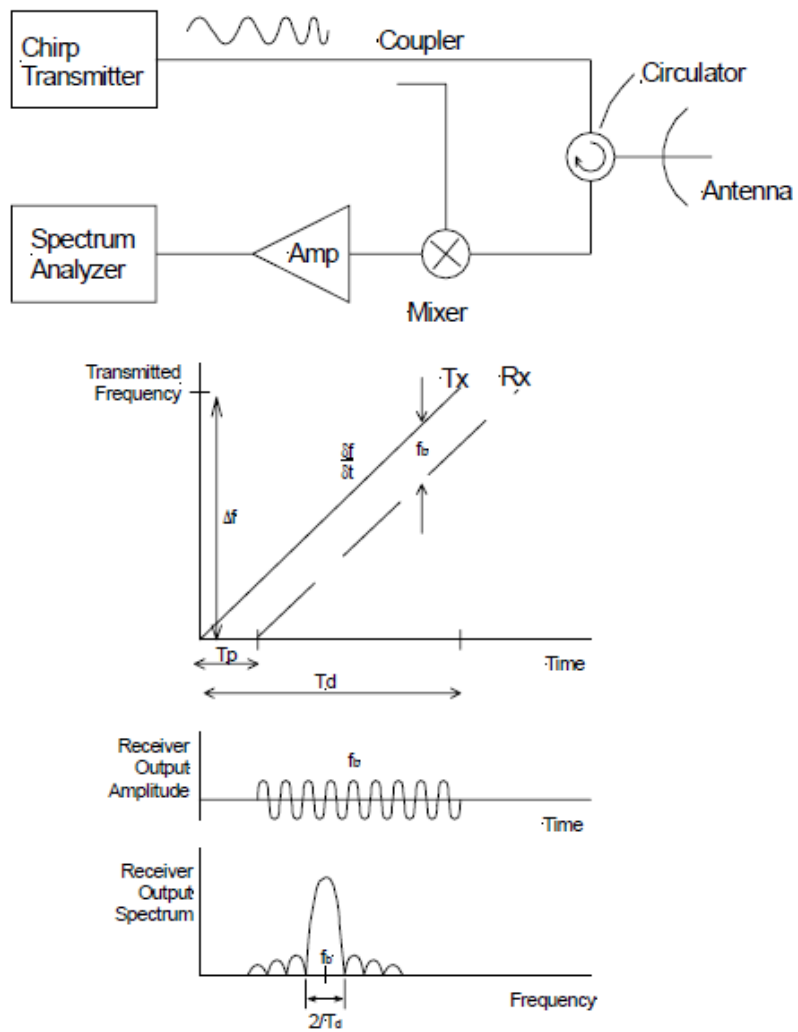
Figure 2.3 FMCW Radar concept.
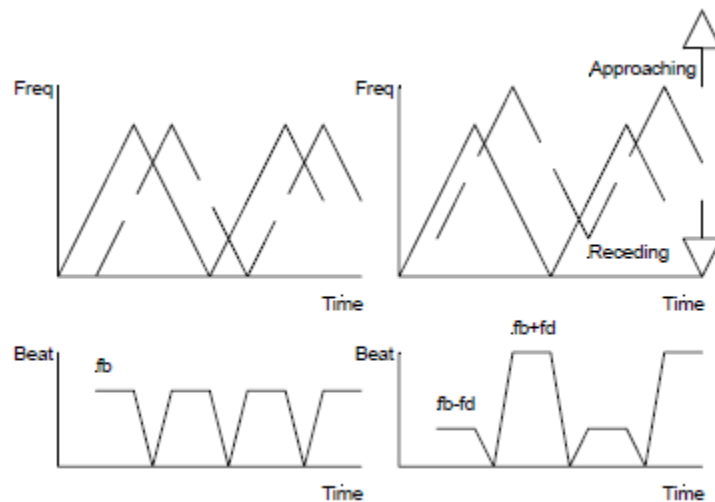
Figure 2.4 Doppler frequency for a moving vehicle in FMCW Radar.

9
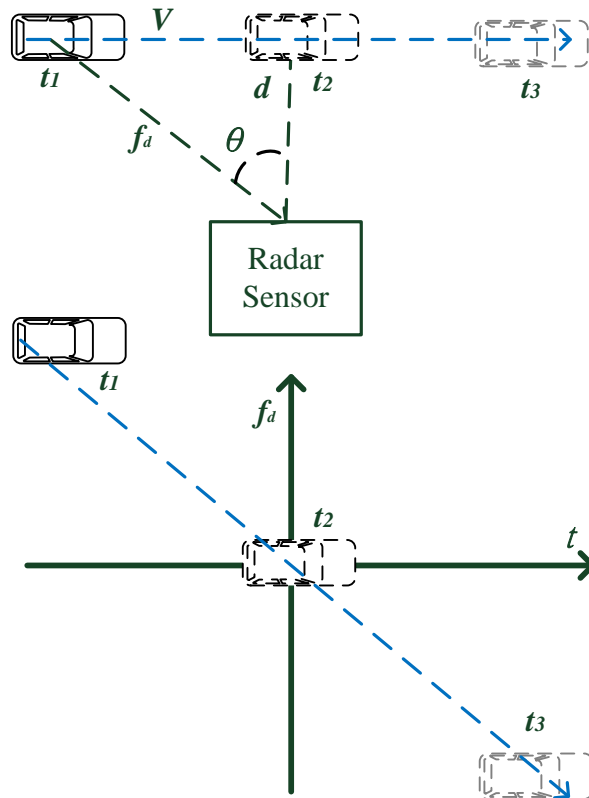
Figure 2.5 Time-frequency distribution of a moving vehicle in FMCW Radar.

The speed of vehicle is calculated as

$$v = \frac{L+L_v}{\Delta t} \ , \tag{2.5}$$

where L is the length of detection zone, L_v is the average effective length of vehicles and Δt is the detector on time. The virtual loop speed can be a good result for average speed. But it is not accurate in general.

Radar and inductive loop detectors have historically performed vehicle classification by providing estimates of vehicle length based on vehicle speed ,v , and the detector on time. The equation for vehicle length, L_v, is given by

L_v=v*on time-effect length of detection zone.

H. Roe and G. S. Hobson (1992) [7] have described a forward-looking FMCW Radar which can separate traffic into five classes. This single lane detector uses the profile of vehicle to do vehicle classification. The profile is formed by the vehicle height and length. The vehicle speed is calculated from Doppler effect. Park et al. (2003) [8] have developed a FMCW side-looking vehicle detection radar. The velocity is estimated by using the appearance duration of the reflected signal and the length of detection zone and Doppler shift. The classification of a vehicle, as large, medium or small size, is possible by processing received power and spectrum pattern

Numerous statistic learning methods have been developed and tested for data cluster or pattern recognition, and these classifiers are categorized into two types: supervised and unsupervised. In supervised learning, the aim is to learn a mapping from the input to an output whose correct vehicle classes are provided by a supervisor. In unsupervised learning, there is no such supervisor and we only have input of data. K-mean cluster is a famous unsupervised classifier that has been used for numerous applications. Furthermore, support vector machine (SVM)[9, 10] and linear discriminated analysis (LDA) [11, 12] are two supervised classifiers. LDA was originally developed in 1936 by R.A. Fisher [13]. SVMs have been used for isolated handwritten digit recognition, object recognition, speaker identification and face detection in images.

K-means is one of the best known data clustering methods. The goal of k-means is to find k points of a dataset that best represent the dataset in a certain mathematical sense. These k points are also known as cluster centers. After obtaining these cluster centers, they can be used for data classification.

LDA is a supervisory classifier. LDA obtains a linear transformation ("discriminant function") of the two predictors, X and Y, which yields a new set of transformed values

that provides more accurate discrimination than either predictor alone. A transformation function is found that maximizes the ratio of between-class to within-class variance. The transformation seeks to rotate the axes so as to maximize the differences between the groups when the categories are project on the new axes. In the ideal case, a projection can be found that completely separates the categories. However, in most cases no transformation exists that provides full separation, so the objective is to obtain the transformation that minimizes the overlap among the transformed distributions. The LDA can be derived as a plug-in Bayes classifier. LDA projects the nine feature dimension space considered in this study into a three dimension linear discriminant (LD) space.   The plug-in classifier finds the average group centers for each vehicle category and saves it. When predicting a test sample vehicle, the classifier measures the Mahalanobis distance between the group center and the LD project point of the vehicle features. The plug-in classifier then estimates the posterior probability of each group using Mahalanobis distance, the prior probability which is the group probability of training set, and the covariance matrix.   The testing vehicle belongs to the group with the highest posterior.

SVM is also a supervisory classifier. SVMs attempt to identify a set of support vectors, two support hyperplanes, and an optimal hyperplane for separating two groups. SVM is a binary classifier. Two strategies can be developed to support multiple classifications: one-against-one and one-against-rest. The one-against-rest strategy constructs k SVMs to separate k groups. The m-th SVM separates the m-th group from the others. For k groups, the one-against-one strategy constructs k(k-1)/2 SVMs to separate each pair of groups.

2.2 Shockwave estimation

The theory of shockwaves had first developed by Lighthill and Whitham[14] . Such shocks are generated at the discharge rates fall due to congestion or the termination of a phase. The shockwave appears due to vehicle speed change, and this configuration is very comprehensive to analyze traffic behaviors. As Figure 2.6 [15], the trajectories of shockwaves were derived by assuming an average arrival rate at the queue tail. It is noted that $y_1(0)$, $y_1(c)$ represent the initial and final queue length and the line A_1, C_1, M_1, D_1, E_1 the trajectory of the queue tail at which a shockwave is formed, l_1 and l_2 are the lost time during phase transitions and g_1 is effective green time. By the shockwave concepts at a signalized intersection, the required green time, queue length and the end time of shockwave are listed as following equations.

The minimal green time for under-saturated approach is

$$g_{lu} = 4(K_j - K_a)^2 (t_{Cl} - l_l) / [(K_j - 2K_a)^2]1) \tag{2.6}$$

The end time of shockwave A_1, C_1 is

$$t_{Cl} = \left\{ K_j \left[\frac{y_l(0)}{u_f} + l_l \right] \right\} / (K_j - K_a)) \tag{2.7}$$

The final queue length for E_1 is

$$y_{El} = y_l(c) = y_l(0) + \frac{K_a u_f c}{K_j} - \frac{K_j g_l u_f}{[4K_j - K_a]} - 2K_a^2 u_f l_l / [K_j - K_a]K_j) \tag{2.8}$$
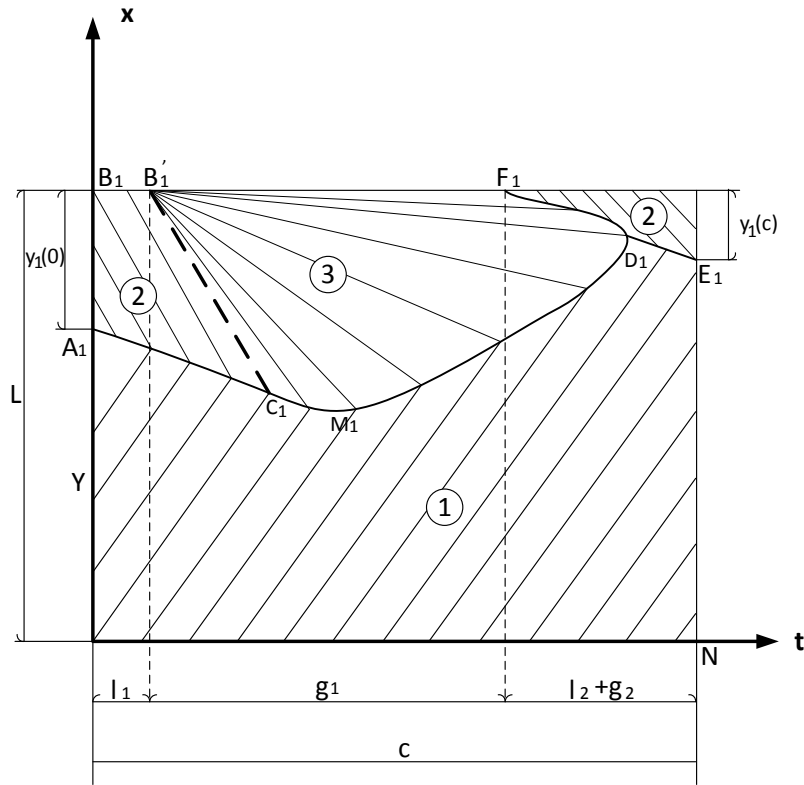
Figure 2.6 Shockwaves at an intersection [15].

A.D. May [16] have analysis the shockwave at signalized intersection as Figure 2.7. A flow-density curve and approaching traffic flow states A, B, C and D are specified. A distance-time diagram is shown in Figure 2.8 so that the slopes WAB, WBC, WAC and WAD in two diagrams represent shockwave speeds. Then, the required green time to discharge the traffic is

$$t_4 - t_2 = \frac{r(W_{AB})}{W_{BC} - W_{AB}} \left(\frac{W_{BC}}{W_{AC}} + 1 \right) \tag{2.9}$$

The maximal queue length is

$$Q_M = \frac{r}{3600} \left[\frac{(W_{BC})(W_{AB})}{W_{BC} - W_{AB}} \right] \tag{2.10}$$

Although some green time and queue length had been explored in the article, the shockwave speeds are calculated by the flow and density difference between flow states.

14
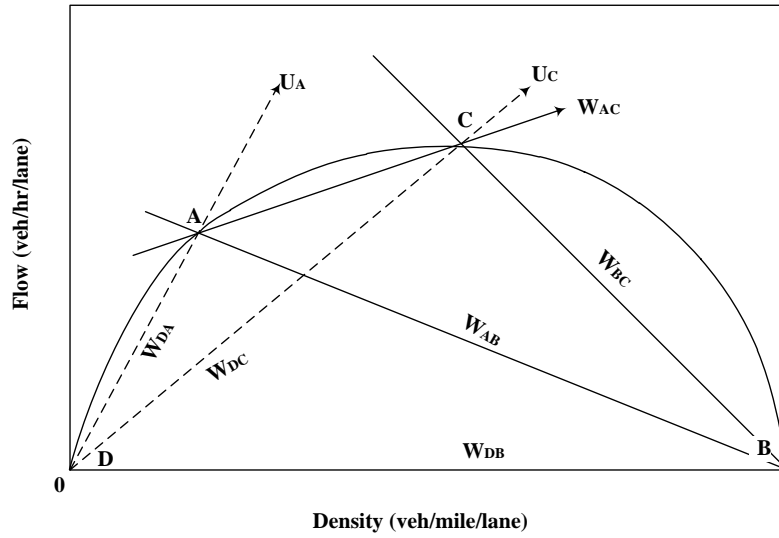
Figure 2.7 Shockwave in flow-density curve[16].
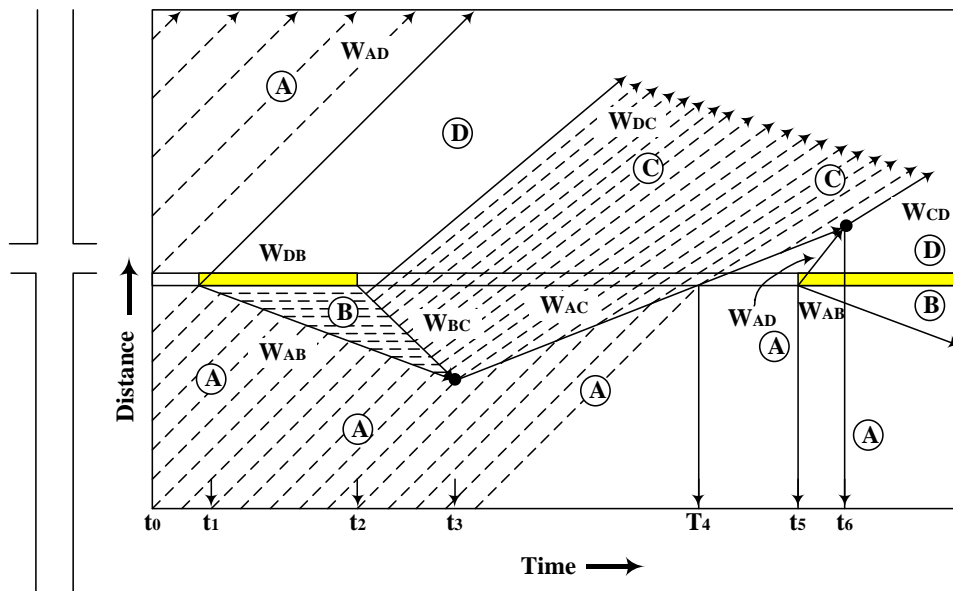
Figure 2.8 Shockwave in time-distance diagram[16].

Instead of counting arrival traffic flow in the current signal cycle, Xinkai et al. (2009)[17] solve the problem of measuring intersection queue length by exploiting the queue discharge process in the immediate past cycle. As Figure 2.9 , the authors find the break points for A, B and C by detector occupancy time, and applying Lighthill–Whitham–Richards (LWR) shockwave theory, the authors are able to identify the change of traffic queue length.
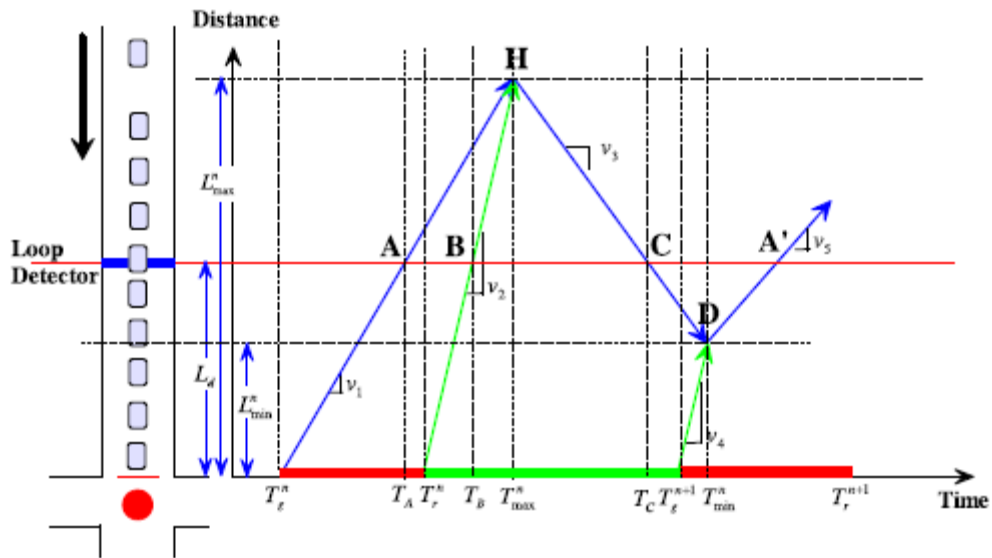
Figure 2.9   Shockwaves and queue length detection in an intersection [17].

Shockwave analysis has long been applied to traffic flows [18, 19]. Shockwaves are defined as boundaries in the time-space domain that indicate a discontinuity in flow-density conditions [16], or the motion of a change in concentration and flow [20]. A typical time-space diagram at a signalized intersection is illustrated in Figure 2.10, where the trajectories of individual vehicles are shown as thin black lines. Three types of shockwaves are represented as thick black line segments: $\overline{EG}$, a backward forming shockwave; $\overline{BG}$, a backward recovery shockwave; and $\overline{GD}$, a forward recovery shockwave [16]. Shockwave analysis can effectively analyze flow and queuing problems [21, 22]; queue can be describe as $\overline{BF}$ and $\overline{CG}$ in Figure 2.10. Researchers have applied shockwaves to compute delay (area *AEGB* in Figure 2.10) and green phase time ($\overline{BD}$ in Figure 2.10) for traffic signals control [23, 24, 25]Numerous schemes have also been proposed for plotting shockwaves and forecasting traffic system performance [18, 21].

Most previous shockwave analyses and applications determine shockwave values

by traditional traffic parameters including volume, speed, and density [22, 26, 23, 25, 27, 28]. While others calculate shockwave by combining gap time, headway and speed [21], or make use of high-resolution vehicle actuation data and signal information [29, 17, 30]. Skabardonis estimates upstream flow with flow, occupancy and phase timing while traffic queue beyond vehicle detector[31] .
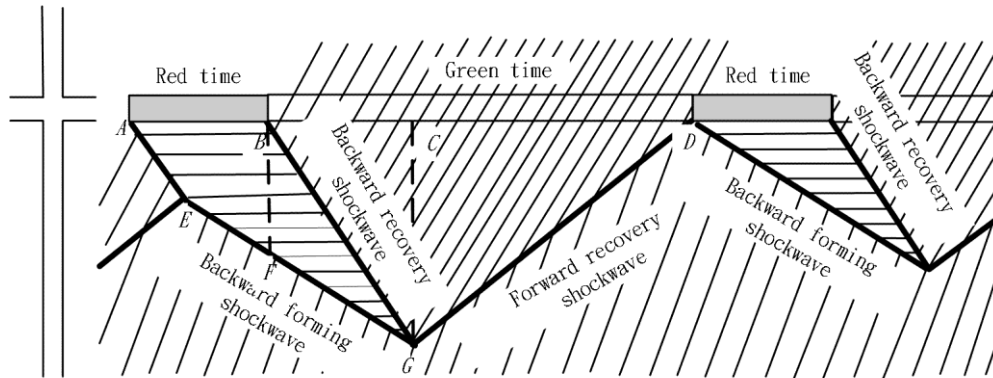
Figure 2.10 Shockwaves in the time-space domain for a signalized intersection.

2.3 Signal control methods

Pre-time signal control

The pre-timed control, which has fixed cycle lengths and preset phase times, operates according to a predetermined time schedule. The pre-timed controllers are best suited for locations with stable volumes and traffic patterns such as downtown areas. Timing plans are usually selected on a time-of-day/ day-of-week basis. Although pre-timed controllers have a degree of flexibility for daily traffic, they can cause excessive delay when the traffic signal controller uses timing plans determined from historical demands.   The Webster method can be used to determine the optimum cycle lengths for minimal delay.

Webster (1958) [32] has shown that minimum intersection delay is obtained when

the cycle length is obtained by the equation

$$C = \frac{1.5L + 5}{1 - \sum_{i=1}^{n} y_i}$$

(2.11)

where:

C = optimal cycle length (second);

L = total lost time per cycle (second);

y_i = the critical lane group volume (i th phase, vph) / saturation flow (vph);

n = number of phases.

The total lost time is the time not used by any phase for discharging vehicles. Total lost time is given as

$$L = \sum_{i=1}^{n} l_i + R$$

(2.12)

where:

l_i = lost time for phase i, which is usually 4 seconds;

R = the total all-red time during the cycle.

The total effective green time, available per cycle, is given by

$$G_{te} = C - L.$$

(2.13)

To obtain minimum delay, the total effective green time should be distributed among the different phases in proportion to their y values to get the effective green time for each phase,

$$G_{ei} = \frac{y_i}{y_1 + y_2 + \cdots + y_n} G_{te}.$$

(2.14)

The actual green time for each phase (not including yellow time) is obtained by

$$G_{ai} = G_{ei} + l_i - \tau_i$$

(2.15)

Where τ_i is yellow time for phase *i*.

Actuated signal control

An actuated signal [33] operates with variable vehicular timing and phasing intervals that depend on traffic volumes. The signals are actuated by vehicular detectors placed in the roadways. The cycle lengths and green times of actuated control may vary from cycle to cycle in response to demands. Actuated controllers include semi-actuated, fully actuated, and density controllers.

In semi-actuated operation, the main street has a "green" indication at all times until a vehicle or vehicles have arrived on one or both of the minor approaches. The signal then provides a "green" phase for the side street that is retained until vehicles are served, or until a preset maximum side-street green is reached. Non-actuated phases may be coordinated with nearby signals on the same route, or they may function as an isolated control. Non-actuated phases usually operate with fixed minimum green times and may be extended by using green time that is not used by actuated phases with low demand. That is, the green duration will be extended beyond the minimum green time until a vehicle actuates the detector on the side street. At a semi-actuated controlled intersection, detectors installed on the side street collect information for timing the signal.

In fully actuated operations, all signal phases are controlled by detector actuations. In general, each phase has a minimum green duration, but it also is shorter than the maximum green time. A phase in the cycle may be skipped entirely if no demand exits for that phase. The right of way does not return automatically to a specific phase under the fully actuated mode unless recalled by a special setting in the controller. That is, the controller shows green indication in the phase last served until conflicting demand appears.

In density operations, the controllers keep track of the number of arrivals and

reduce the allowable gap according to several rules as vehicles show up or as time progresses. The specifications allow gap reduction based only upon time waiting on the red. This type of controller also has a variable initial interval, thus allows a variable minimum green. Detectors are normally place farther back of the intersection stop line, particularly on high-speed approaches to the intersection of major streets.

The timing characteristics of actuated signal operation are introduced here. In an actuated phase, there are three timing parameters: the minimum green interval, the unit extension, and the maximum green interval. These intervals are a function of the type and configuration of the detectors installed at the intersection. These three intervals are shown in Figure 2.11. This figure shows a case that the phase terminates before it reaches the maximum green period because there is no vehicular actuation in the last unit extension period.

The unit extension is time by which a green phase could be increased during the extendable portion after an actuation on that phase. It depends on the average speed of the approaching vehicles and the distance between the detectors and the stop line.

Initial interval is the first portion of the green phase that is adequate to allow vehicles waiting between the stop line and the detector during the red phase to clear the intersection. This time depends on the number of vehicles waiting, the average headway, and the starting delay.

The minimum green interval is the shortest time that should be provide for a green interval during any traffic phase. In basic design of actuated phase intervals, the minimum green interval equals the sum of the initial interval and the unit extension.
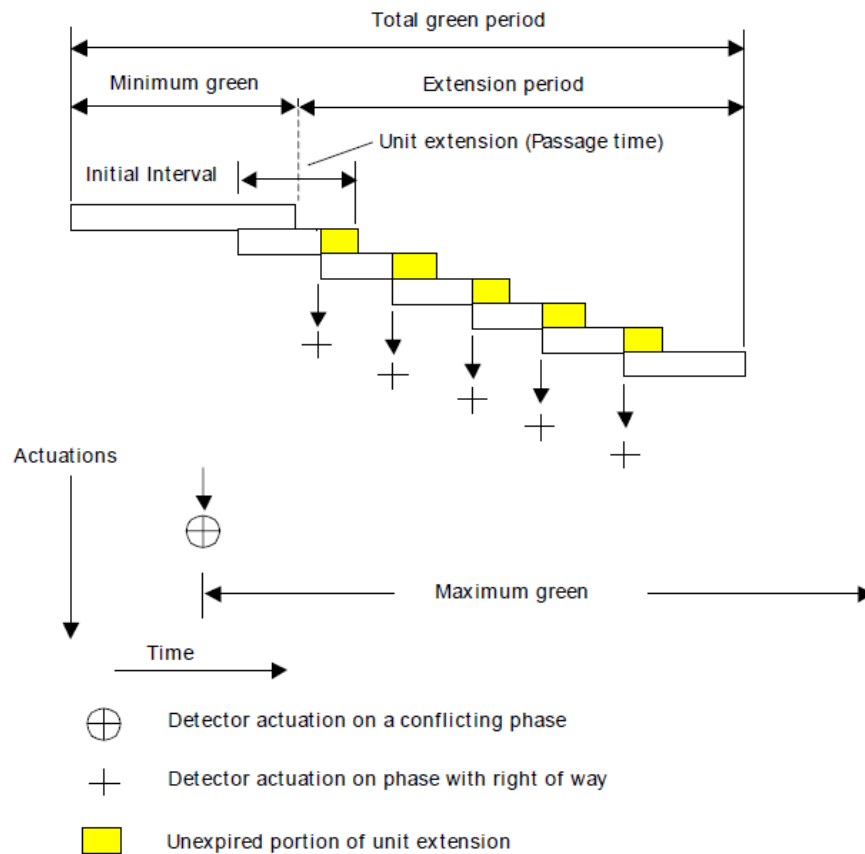
Figure 2.11 Actuated phase intervals

The maximum green interval is the limit that a phase can hold green in the presence of conflicting demand. Normal range of maximum green is between 30 and 60 seconds depending on traffic volumes. Webster's model for pre-timed controllers can be used to compute the maximum green interval. The computed green intervals are multiplied by a factor ranging between 1.25 and 1.50 to obtain the maximum green.

Traffic-actuated controllers automatically determine cycle lengths and phase durations based on detection of traffic on the various approaches. The cycle lengths and green times are random variables, which depend on the real-time traffic demand. Therefore, the capacities of approaches to an intersection are random variables.

Synchro software

Synchro [34] is a macroscopic and deterministic signal timing tool. Synchro has the following features: it is able to simultaneously optimize lead-lag phase ordering in addition to cycle lengths, phase lengths, and coordinated offsets, Percentile Delay estimation method, data input and comprehensive output options, capability of modeling RTOR, U-turns and six-legged intersections, capability of modeling signalized and signalized intersections and roundabouts and it allows exporting its files to CORSIM and HCS.

Synchro implements the HCM 2000 procedures for signalized intersections capacity and delay calculation. Also, it possesses percentile delay calculation method and intersection capacity utilization (ICU) 2003 methods. The basic premise of the percentile delay method is that traffic arrivals follow a Poisson distribution. The percentile delay method calculates vehicle delays for five different scenarios (i.e., 10th, 30th, 50th, 70th and 90th percentiles) and takes a volume weighted average of delays predicted for each scenario. The ICU method sums the amount of time required to serve all movements at saturation for a given cycle length. It is similar to taking sum of critical volume to saturation flow ratios (v/s), yet allows minimum timing to be considered. The ICU can tell how much reserve capacity is available or how much the intersection is overcapacity.

Synchro does not use the Genetic Algorithm for optimization of signal timings. The optimization objective function available is minimizing the percentile delay. It optimizes the four signal timing parameters by evaluating a series of cycle lengths, applying a heuristic method for green splits, conducting an exhaustive search for left-turn phase position and a quasi-exhaustive search for offsets.

The best cycle length is found by calculating a performance index (PI).

The PI is calculated as follows.

$$PI = \frac{D + ST*10 + QP*100}{3600} \qquad (2.16)$$

where

PI = Performance Index;

D = Percentile Signal Delay (s);

QP = Queue Penalty (vehicles affected);

ST = Vehicle Stops (vph);

$$D = \frac{VD10 + VD30 + VD50 + VD70 + VD90}{(vd10 + vd30 + vd50 + vd70 + vd90;)*c/3600};$$

$$VD10 = 0.5 * \frac{v10}{\left(1 - \frac{v10}{s}\right)*3600} * \frac{R^2}{c} * 3600;$$ VD10 = 10th percentile Vehicle-Delay per

hour;

v10 = 10th percentile volume rate (vph).
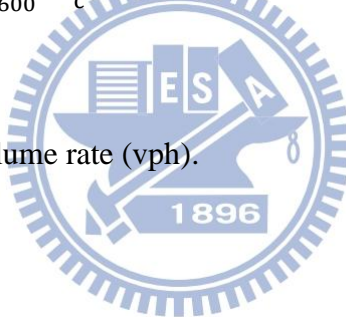
TRANSYT 7F

TRAffic Network StudY Tool (TRANSYT) is one of the most widely used signal timing programs. The original version of TRANSYT was developed by Dennis Robertson at the Transportation and Road Research Laboratory in UK in 1967. Though TRANSYT is most commonly used as an offline optimization tool, it may also be used in an online fashion to compute signal settings every few minutes and download these settings to the field. TRANSYT is a macroscopic, deterministic simulation and optimization model. The model requires the link flows and link turning proportions as inputs and assumes them to be constant for the entire simulation period. The program optimizes splits and offsets given a set cycle length and carries out a series of iterations between its traffic simulation module and the signal setting optimization

23

module. TRANSYT-7F (Traffic Network Study Tool, version 7, Federal) [35] was "Americanized" for the Federal Highway Administration (FHWA) in 1981 by the University of Florida Transportation Research Center. TRANSYT-7F Release 10.1 introduced in January 2004 included the ability to optimize cycle length, phase sequence, green splits and offsets using a genetic algorithm (GA) and a traditional hill-climb technique. Recent versions of TRANSYT-7F introduced the CORSIM simulator in its optimization of cycle length, green splits and offset only. The direct-CORSIM optimization in T7F consists of the CORSIM simulator and the GA optimizer. It uses the CORSIM input file (*.trf) as an input so that T7F can directly import all information related to the network and signal timing plan from the CORSIM input file.

TRANSYT-7f includes detailed simulation of platoon dispersion, queue spillback, queue spillover, traffic-actuated control, and the flexibility to perform lane-by-lane analysis. Beside link wise simulation, TRANSYT-7F provides stepwise simulation which updates all links one time step at a time. With stepwise simulation, TRANSYT-7F can explicitly model queue spillback condition. TRANSYT-7F provides left-hand drive right-hand drive option and it can only simulate two-way stop-controlled (TWSC) intersections. HCS files can be loaded directly into T7F and timing plans can be exported from T7F to HCS. Many traffic principles embedded in TRANSYT-7F such as arrival type, delay calculation, level of service, capacity calculation and saturated flow calculation are based on HCM 2000 procedures. TRANSYT-7F includes measures of effectiveness (Throughput) for use in optimization of congested networks. TRANSYT-7F has twelve distinct criteria. These criteria include functions designed to minimize delay, minimize a combination of delay and stops (the Disutility Index-DI), maximize progression opportunities (PROS) and maximize throughput among others.

The performance index (PI) may be defined as follow:

$$PI = \begin{cases} DI \text{ only} \\ PROS \text{ only} \\ PROS \ \& \ DI \\ PROS/DI \\ DI * \sum_i \dfrac{\text{Average Back of queue on link i}}{\text{Queue capacity on link i}} \\ \text{Throughput only} \\ \text{Throughput} \ \& \ DI \\ \text{Throughput/DI} \end{cases} \tag{2.17}$$

MAXBAND

In 1966, John D. C. Little and his research colleagues at MIT defined the new state of the art, called MAXBAND[36, 37, 38], ending with a set of algorithms to synchronize fixed-timed traffic lights for streets with two-way traffic. It is one of the representatives of the Fixed-Time Coordinated Control Strategies. By their nature, fixed-time strategies are only applicable to under-saturated traffic conditions.

MXBAND considers a two-way arterial with n signals from S_1 to S_n (intersections) and specifies the corresponding offsets in order to maximize the number of vehicles traveling at given range of speed without stopping at any signal (green wave). MAXBAND considers splits as given (in accordance with the secondary street demands); hence the problem consists in placing the known red durations of the arterial's signals to maximize the inbound and outbound bandwidths In_B and Out_B, respectively (See Figure 2.12). In order to make MAXBAND work for a network of arterials, Little (1966) extended the basic MAXBAND method by incorporation of some cycle constraints. MAXBAND used into several networks into North America and other countries.

25
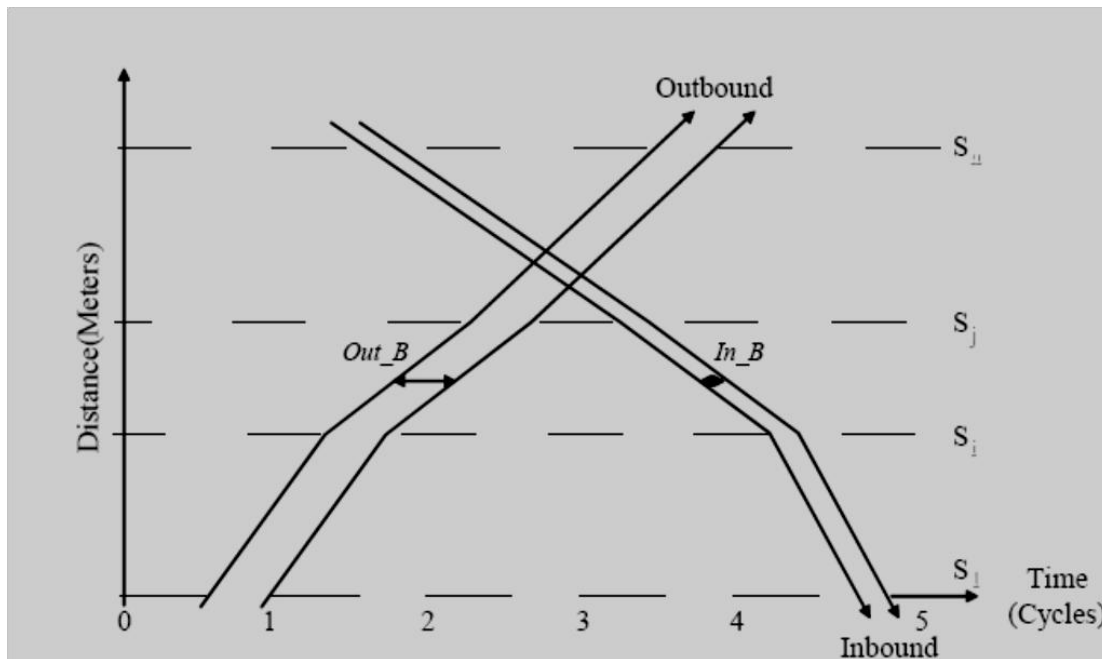
Figure 2.12 A maximum band along an arterial [36].

The underlying optimization model in MAXBAND is a Mixed Integer Linear Programming (MILP) model. MAXBAND include its freedom to provide a range for the cycle time and speed and it can operate a traffic signal effectively through the interlocking control of neighboring intersections. Its disadvantages are the lack of incorporated bus flows, limited field tests and because it is based on off-line analysis, it is impossible for it to cope actively with irregularities in the traffic environment. MAXBAND optimizes the signal by maximizing arterial progression bandwidth.

The output of the program includes cycle time, offsets, speeds and order of left turn phases to maximize the weighted combination of bandwidths. The program can automatically choose cycle time from a given range, allow the design speed to vary within given tolerances, select the best lead or lag pattern for left turn phases from a specified set, allow a queue clearance time for secondary flow accumulated during red, accept user-specified weights for the green bands in each direction and handle a simple

26

network in the form of a three artery triangular loop.

The limitation of Maximization existing bandwidth is that the progression bands do not correspond to the actual traffic flows on the arterial links. Therefore, bandwidth maximization will not always lead to optimal system performance in terms of stops, delay, and fuel consumption.

Near researches

The jammed traffic of closely spaced intersections is generally derived from poor progression, unstable demands and inefficient signal operation. Poor regression of the signals leads to queue spill-back from one intersection to upstream intersections. To solve the aforementioned problems, researches focused on oversaturated demand, closely spaced intersections, and traffic flow theories should be considered together. Abu-Lebdeh and Benekohal [23] had developed a traffic control method and queue management procedures for oversaturated arterials. Chang and Sun [39] had optimized an oversaturated network by utilizing a bang-bang like model for the oversaturated intersections and TRANSYT-7F for the undersaturated intersections. Michalopoulos and Stephanopoulos brought the concept of shockwave theory to traffic signal control [29]. Tian, Urbanik and Gibby [40] had an application of diamond interchange control strategies on a site of six closely spaced intersections. Messer [41] had studied the traffic operations at oversaturated, closely spaced signalized intersection by NETSIM simulations. Liu and Chang [42] had an arterial signal optimization model to do with queue spill-back and lane blockage. Existing researches usually paid attention to through traffics of the arterial; however, they seldom focused on the crooked traffics of the adjacent minor approaches. As the traffic demand on minor approaches grows, progression on those approaches should also be introduced. Despite the contribution of those researches, most of such models have not addressed such progression issue.

Existing full-actuated signal scheme can only be applied to arterials; not much it can do while facing a path-based progression situation. Zheng and Chu [43] and Skabardonis [31] suggest methods to dynamically adjust maximal green for full-actuated control under oversaturated traffic. With adjustable maximal green, full-actuated control scheme have the potential to adaptive to oversaturated demands. However, full-actuated schemes are focused on approach or arterial; they never focused on path-based progression. Therefore, they should be modified to suit the specific path-based situation.
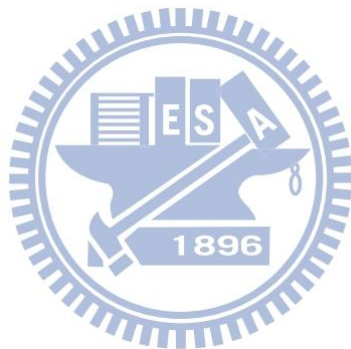
III. Research methodology

In this chapter, some essential concepts of the critical path signal control of closely spaced intersections are discussed. Begin with the introduction to Radar vehicle detection algorithm, the brief introduction to three new traffic parameters is addressed in section 3.2. Section 3.3 shows the shockwave detection at intersection. The estimation for upstream flow and speed by shockwave concept is illustrated in section 3.4.   A critical path signal control algorithm is introduced, in section 3.5.

3.1 Radar vehicle detection algorithm

The radar cross section (RCS) of a vehicle is the key information used in vehicle classification and speed estimation. Figure 3.1 shows a sample RCS signal of a car received from the installation of Figure 3.1(a). The closed area indicated by a dashed line is the detection area of the radar detector. The profile of a vehicle signal resembles a mountain, and different vehicles create different shaped mountains. The vehicle classifier extracts features from the profiles and classifies vehicles accordingly.

The speed estimator also identifies features from the profiles and calculates the vehicle speed. Vehicle RCS is influenced by radar height and angle, radar distance from the first lane, vehicle speed, vehicle shape and vehicle distance to radar. Most of these factors are only fixed on the completion of radar sensor installation. Restated, the vehicle profiles were completely changed when the environmental installation was adjusted. This is a constraint for the supervised classifier, which needs to be retrained for each new environmental installation. Generally, traffic managers hope that sensor setup minimally impacts traffic condition. It means that the sensor setup time must be minimized. The setup time influences the learning time and learning data of a classifier.

If a training classifier is provided, the learning data is gathered during setup. Short setup time results in a skewed distribution of vehicle types. The number of cars may be large while the number of trucks is few. This forms the second constraint: short training time and skewed training data.
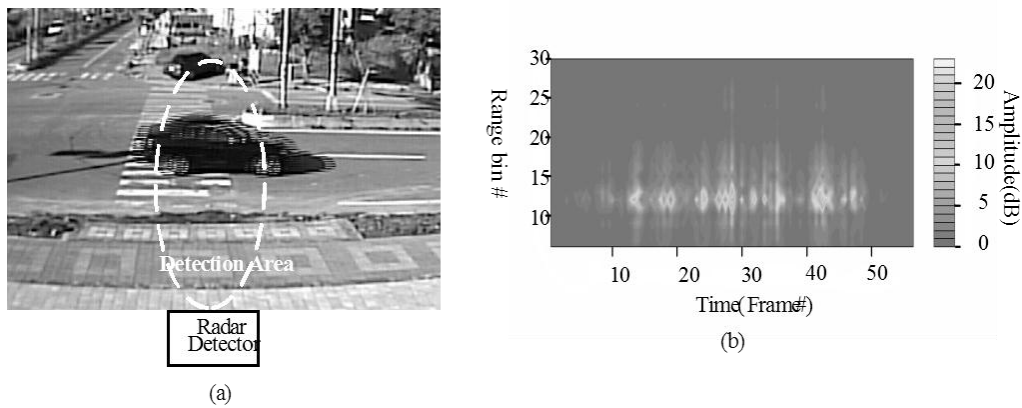
Figure 3.1 (a) A picture of a vehicle passing through the detection area of a radar detector.　　(b) The spectrogram of the vehicle shown in Figure (a).

Figure 3.2 presents a flowchart of an algorithm for these two constraints. The algorithm includes four phases, namely signal processing, calibration, learning and 'classification and speed estimation'. The rectangles which are enclosed by a dashed line comprise four major phases: signal processing, calibration, learning and 'classification and speed estimation'. After retrieving the radar signal, a high pass filter is applied to filter background clutter signals.　　Fast Fourier transformation is to get the range profiles of vehicles on lanes. Then, a constant false alarm rate (CFAR) thresholds are used to detect the presence of vehicles. If the calibrating work is needed, the video calibrating system will be used to calibrate the virtual loop lengths. When the calibrating job is finished, the vehicle profiles will be complemented by the range of vehicle. The aim is to let vehicles have the same signal gains in different lanes. The next

step is to extract nine features from the complemented vehicle profile. While the training job has never been done before, these features will be saved in vehicle training database. The category and length of vehicle, which is the output of video recognition system, will be saved into training database, too. If the number of vehicles is bigger than a threshold, SVM and SVR will finish the learning step. When the learning job is done, SVM will use vehicle features to classify vehicle's category. Finally, SVR will predict the length of vehicle and output the vehicle speed. The details of the algorithm will be presented in following subsections. The pseudocode of algorithm is shown as following.
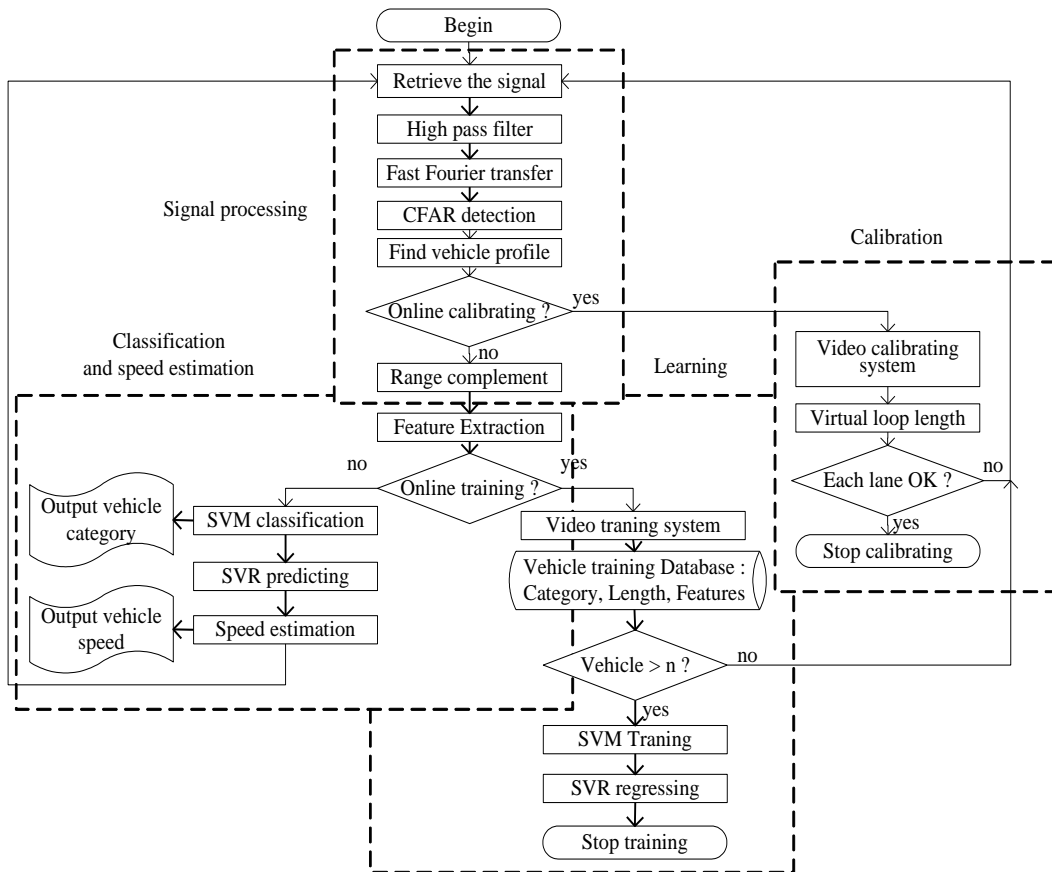
Figure 3.2 The flowchart of the vehicle detection algorithm.

```
Void Vehicle_classifier_and_speed_estimation_algorithm()

begin

while true

                Signal_processing();

                if need calibrating

                    Calibrating();

                endif

            if vehicle<n

                    Feature_extracting();

            endif

            if need training

                    Learning()

              endif

            if training done

                Vehicle_classification_and_speed_estimation();

            endif

        endwhile

End


void Signal_processing()

begin

retrieve signal from system;

            apply high pass filter;

            do fast Fourier transform;

             find threshold   by clutter-map CFAR;
```

find vehicle profile;

end

void   Calibrating()

begin

    for each lane of street

        check vehicle in/out by vehicle profile and   clutter-map CFAR threshold

            if vehicle-in

                capture vehicle-in image from video

             endif

             if vehicle-out

                capture vehicle-out image from video

                compute virtual loop length by vehicle-in-out images

                classify vehicle category by images

                compute vehicle length by images

                compute speed

                save above results into training database

             endif

          endfor

end

void Feature_extrating()

begin

    if   vehicle-out

        compute   energy   of   vehicle profile

33

compute square energy

compute sum,maximal, mean and mean square error of vehicle
magnitude profile

compute vibration of vehicle profile

compute square vibration

save all features into database

endif

end

void Learning( )

begin

retrieve vehicle features from database

retrieve vehicle length, speed, type, and loop length from database

do SVM training

do SVR regression

end

void vehicle_classification_and_speed_estimation( )

begin

do vehicle classification by SVM

do vehicle length prediction by SVR

estimate vehicle speed

end
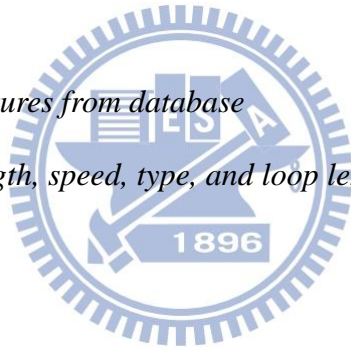
Signal processing

Most of the signal processing is performed during this phase. A discrete signal frame $x_t[n]$ is retrieved from the time domain during a pulse interval t. Each discrete signal frame has 128 points (n=1..128), and there are a total of 1500 signal frames per second (pulse repeating frequency =1500). Since noise and background clutter disturb normal vehicle echo signals, a simple high pass filter $H(z)=1-z^{-1}$ is used to cancel the background clutter. The filtered signal $y_t[n]$ is shown in Eq. (3.1).

$$y_t[n]=x_t[n]-x_{t-1}[n] \tag{3.1}$$

Furthermore, the high pass filter can also emphasize the moving of vehicles. Since a high magnitude of some frequencies means that some vehicles present on some lanes, fast Fourier transform (FFT) is performed on $y_t[n]$ to get the frequency domain data $Y_t[n]$. That is to say, when a vehicle is presented at distance 3*n meters at time t, $|Y_t[n]|$ is great than some threshold. To avoid false alarms of vehicle presence, the clutter-map constant false alarm rate (CFAR) [44] technique is adopted. The basic characteristic of clutter-map CFAR is that the false alarm probability remains approximately constant in clutter by a dynamic threshold. Vehicles with an echo power exceeding the threshold thus can still be detected. Eq. (3.2) shows the clutter-map CFAR threshold for the range n during pulse t.

$$T_t[n] = \alpha(\gamma \times |Y_{t-1}[n]| + (1-\gamma) \times |Y_{t-2}[n]|) \tag{3.2}$$

where α =2 and γ =0.9.

The final step in signal processing is to collect the vehicle profile $V_t[m]$ presented at m-th range bin $Y_t[m]$ during the time interval in which vehicle is presented on detection area. All classification methods are based on the vehicle profile from which features are extracted. Eq. (3.3) defines the profile of the vehicle signal. Each magnitude of m-th range bin $|Y_t[m]|$ is multiplied by power k of range frequency f_m to compensate for the decay of received power.

$$V_t[m] = |Y_t[m]| \times f_m^k \qquad (3.3)$$

where $T_1 < t < T_2$ and T_1 and T_2 are the first and last detection times of a vehicle which passes through the radar detection area.

Feature Extraction

Nine features need to be extracted from the vehicle profile, most of which are based on the physical characteristics of the vehicle. First, the energy of the vehicle profile is shown in Eq. (3.4). A large vehicle implies large RCS, which in turn means high energy. Square energy is used to emphasize this characteristic. Other features are obtained from the statistical parameters associated with the vehicle magnitude profile. These features include the maximal, mean and mean square error for elements of $V_t[m]$.

$$Energy = \sum_{t=T_1}^{T_2} V_t(m) \qquad (3.4)$$

Another physical phenomenon of vehicles is the vibration of the vehicle profile. Small vehicles have low vibration while large vehicles have high vibration. Eq. (3.5) calculates vehicle vibration. To increase the weighting of these characteristics, the square of vibration is used. The vibration is just like to do mathematical differentiation

and the energy is the same concept as doing mathematical integration. These features of each vehicle profile form a point in the feature space.

$$Vibration = \sum_{t=T_1}^{T_2} |V_t(m) - V_{t-1}(m)|$$

(3.5)

Learning and Classification

This section aims to identify a classifier for effectively classifying vehicles into one of four categories: motorcycles, small, medium and large.

First, this study tries the K-means clustering (denoted as K-means). Here K-means is used as a method of partitional clustering in which the numbers of clusters and random centers are specified before starting the clustering process. The number of clusters is set to four. An objective function is then defined as the sum of the square distances between a point in a feature space and the nearest cluster centers. The standard K-means procedure is then followed to minimize the objective function iteratively by finding a new set of cluster centers. These cluster centers can reduce the value of the objective function at each iteration. Here the maximal iteration is set to 10.

The next classifier is LDA, which is a supervisory classifier. LDA measures the Mahalanobis distance between the group center and the LD project point of nine vehicle features. The LDA then estimates the posterior probability of each group using Mahalanobis distance, the testing vehicle belongs to the group with the highest posterior.

The last classifier is SVM, which is also a supervisory classifier. SVM is a binary classifier. The one-against-one strategy is developed to support multiple classifications For k groups, the one-against-one strategy constructs $k(k-1)/2$ SVMs to separate each pair of groups. This study tests SVM using the one-against-one approach, in which six SVMs are constructed, each of which trains data from two different vehicle groups.

Prediction is performed by voting, where each classifier makes a prediction and the most frequently predicted class wins ("Max Wins"). In cases where two groups receive an identical number of votes, this study simply selects the one with the smallest index.

For supervisory classifiers LDA and SVM, the environmental installation problem leads to retraining of the classifier for each installation of radar sensors. To resolve the problem, this study proposes a learning method based on a video training system, as shown in Figure 3.3. The system receives vehicle-in and vehicle-out triggers when a vehicle is either inside or outside the detection area. After receiving the triggers, the system captures two video frames. The image processing unit then outputs virtual loop length, vehicle category and vehicle length. Using clutter-map CFAR, the radar system can know the in and out time of a vehicle. When the radar system sends vehicle-in or vehicle-out triggers to the video system, the video system immediately captures a video frame. These two video frames can then be used to perform image processing to obtain the vehicle type. The vehicle type and its features are saved in a training database which can be used to train a supervisory classifier.
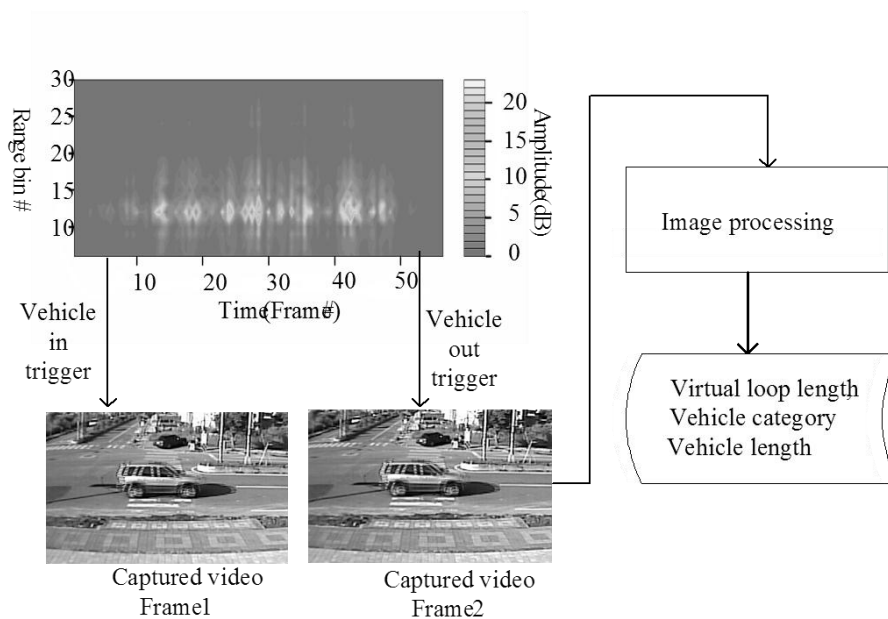
Figure 3.3. Video training and calibrating system.

Calibration and speed estimation

In general, the radar speed detecting method is based on the Doppler principle. When a radio wave bumps onto a tracked object, the radio wave is reflected, the frequency and the amplitude of the reflective wave are influenced by the moving state of the tracked object. If the tracked object is stable in its position, the frequency of the reflective radio wave will not be changed and the Doppler effect will not be generated. If the tracked object moves forward in the transmitted direction of the radio wave, the frequency of the reflective radio wave will be increased; on the other hand, if the object moves oppositely to the propagated direction of the radio wave, the frequency will be decreased. As a result, the effects of the Doppler Shift are produced. However, the Doppler effect is not obviously and stable for roadside fired Radar. It is almost zero when vehicle pass through the detection zones. The RCS of vehicle is so complicated such that equations 2.2-2.4 are not possible to be applied.

Hence, the vehicle speed is estimated using Eq. (3.6). The detection zone of each lane forms a virtual loop. The key to correctly estimating the speed is to more precisely calculate the three parameters of Eq. (3.6).

$$Speed = \frac{L_v + L_z}{\Delta T} \, , \tag{3.6}$$

where L_v denotes the length of the vehicle, L_z represents the length of the virtual loop and ΔT is the time of vehicle occupation.

It is easy to obtain the vehicle occupation time ΔT from clutter-map CFAR. The length of the virtual loop L_z must be carefully calibrated. The length of the virtual loop is also an environmental installation problem. The length differs between environmental installations. Theoretically, the virtual loop length can be obtained from radar equations, antenna patterns, and the height and angle of the radar sensor. However, these

methods are imprecise and inconvenient. A more accurate method is to take measurements in the field. Figure 3.3 presents a video calibrating system for measuring the virtual loop length via image processing. Based on clutter-map CFAR, the times at which the vehicle is either in or outside of the virtual loop can be derived. The video calibrating system can obtain video frames at both in and out time. Image processing can be performed to obtain the distance of vehicle movement between the two frames. The moving distance exactly equals the virtual loop length. SVR is used to estimate the vehicle length L_v. SVR is almost the same as SVM, with one difference being that the optimal hyperplane is used to predict values in SVR, while in SVM it is used to separate classes. Since SVR is still a supervised regression method, the video system is still required to measure the vehicle lengths and save them in the training database.

3.2 Three new traffic parameters

This subsection introduces the definition of traffic parameters including stopped duration, moving duration, and empty duration. A typical time-space diagram of signalized intersection is shown in Figure 3.4, with the vehicle trajectory is indicated as black lines. The traffic parameter, stopped duration, is defined as the vehicle presence at detection zone for an extensive period (for example, 3 seconds for cars and 10 seconds for trucks) of time; while moving duration is defined as the vehicle presence less than that period. The parameter, empty duration, represents no vehicle presence at that period. To improve accuracy, multiple detectors can be used to check whether a vehicle is stopped or not. The stopped duration can also be obtained when the speed equals zero.
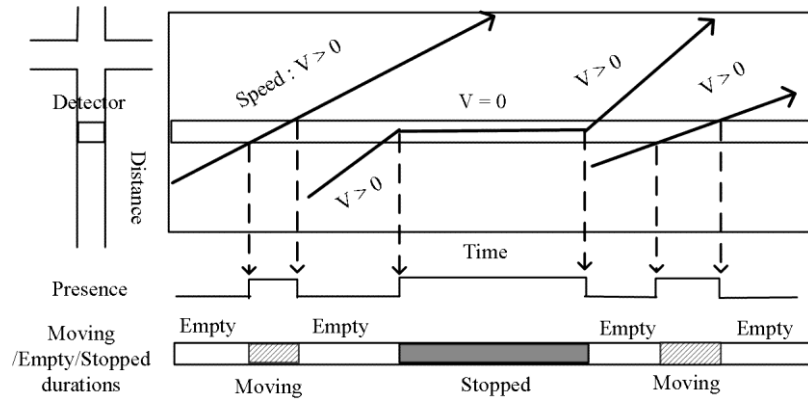
Figure 3.4 Moving duration, empty duration and stopped duration.

3.3 Shockwave detection

This subsection introduces the estimation of shockwave from vehicle detector data. The shockwaves for a signalized intersection is shown in Figure 3.5. Gray lines represent the trajectories of individual vehicles, while black lines or black dash lines indicate shockwaves. This study defines four dedicated flow states. First, flow state 0 (⓪ in Figure 3.5) represents a traffic state with maximal density and the speed equals zero. Second, the flow state 1 (① in Figure 3.5) represents the maximum flow state (defined as flow equals saturated flow rate). Third, flow state 2 (② in Figure 3.5) is defined as the ideal traffic flow, which means vehicles arrive within a cycle equals the saturation flow of green phase. Fourth, flow state 3 (③ in Figure 3.5) is defined as the uniformly distributed flow over a cycle, which might be different from cycle to cycle.

There are three shockwaves among states 0, 1, and 2; W_{20} is defined as ideal backward forming shockwave, W_{21} is defined as ideal forward recovery shockwave, and W_{01} represents a backward recovery shockwave. Figure 3.5(b) demonstrates a similar situation as Figure 3.5(a) but with higher arrival rate (as state 3). Among state 0, 1, and 3, we have shockwaves of 1) W_{30}, a backward forming shockwave, 2) W_{31}, forward recovery shockwave, and 3) W_{01}, a backward recovery shockwave. Moreover, it can be

observed in Figure 3.5(b), where state 3 has a higher arrival rate than state 2, the propagation speed of shockwaves W_{30} would be greater than W_{20} and the speed of W_{31} would be slower than W_{21}. Figure 3.5(c) and 3.5(d) show the relationships among five shockwaves on the fundamental diagram and the time-space diagram.
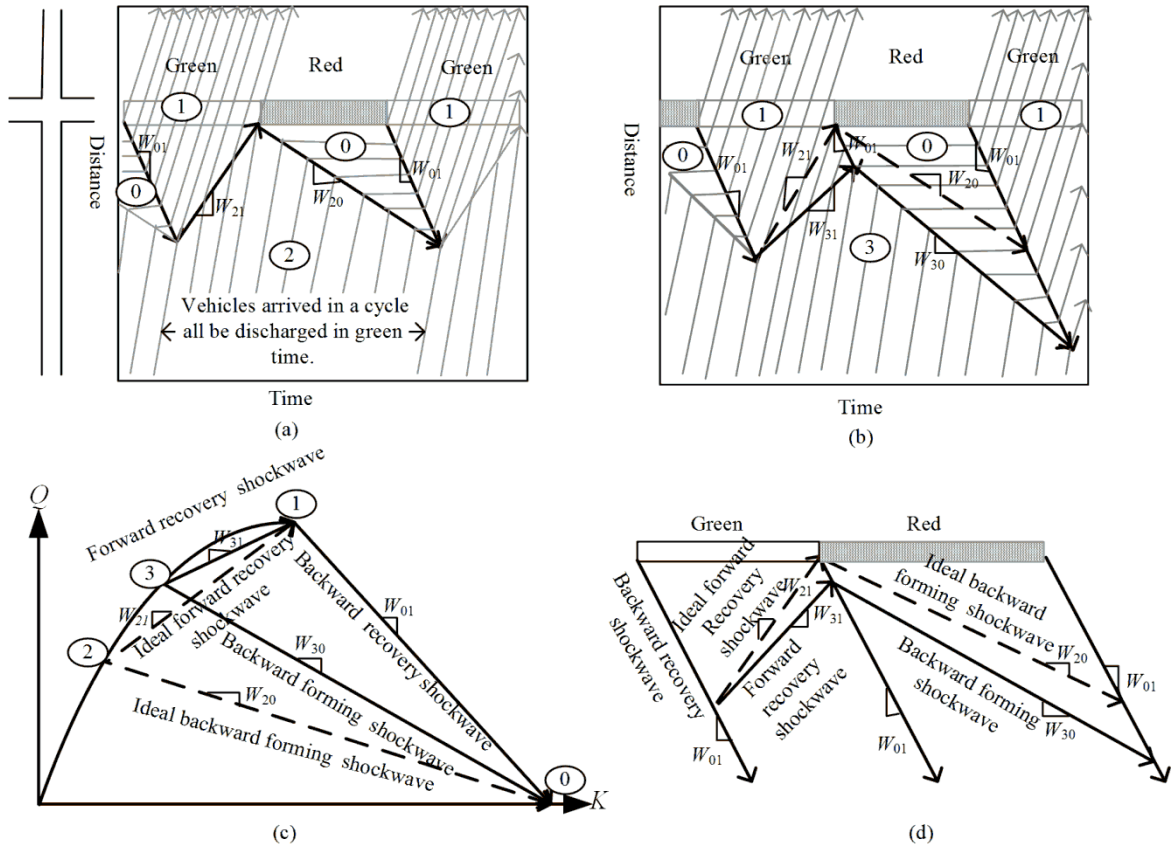
Figure 3.5. (a) Ideal shockwaves for a specified green and red time. (b) Comparison between the ideal shockwaves and general shockwaves. (c) Five shockwave relations in the proposed model. (d) Five shockwaves relations in time-space diagram.

Relationships among shockwaves, speeds and flows

This subsection gives a preliminary understanding of relationships among shockwaves, speeds and densities, and the notations would be used throughout this article. Since the backward moving shockwaves are much slower than the forward

moving shockwaves, this study utilizes an asymmetric fundamental diagram that comprise a parabolic non-congested part and a linear congested part. The proposed stream flow diagram is demonstrated in Figure 3.6. Let flow, density, and speed under flow state x (ⓧ in Figure 3.6) be denoted as Q_x, K_x, and U_x, respectively. The flow state 0 (⓪ in Figure 3.6) is defined as the state of jam density K_j; while the flow state 1 (① in Figure 3.6) is defined as the state which has the maximal flow rate Q_m and density K_m. The maximal flow rate Q_m also represents the saturation flow rate of green phase at a signalized intersection. With proposed flow model, we have $Q_0 =0$ and $K_j =aK_m$, where a is a constant needs to be calibrated. If the real traffic flow can be represented as the Greenshields' model, which is symmetric on both non-congested and congested part, the constant a equals 2. Since backward moving shockwaves are much slower than forward moving shockwaves, the constant a should be greater than 2. For example, with the asymmetric Greenberg's model, the constant a is equal to nature base of logarithms e (2.718).
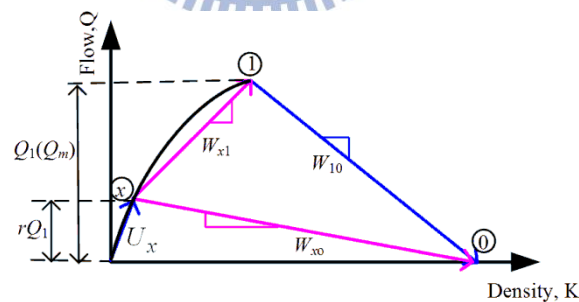
Figure 3.6 The relation between shockwaves

With a flow state x, the speed of shockwaves among different states can be graphically seen in Figure 3.6; while W_{01} denotes the shockwave between state 1 and 0, W_{x1} is the shockwave between state x and 1, and W_{x0} is the shockwave between state x and 0. Throughout this article, W represents the shockwave speed.

The W_{01} can be calculated as

$$W_{01} = \frac{Q_0 - Q_1}{K_0 - K_1} = \frac{-Q_m}{(a-1)K_m} .$$
(3.7)

The W_{x0} and W_{x1} can be calculated as some ratio of the W_{01} by using the following equations.

$$W_{x1} = \frac{Q_x - Q_1}{K_x - K_1} = \sqrt{1-r} \frac{Q_m}{K_m} = (1-a)\sqrt{1-r} W_{01},$$
(3.8)

$$W_{x0} = \frac{Q_x - Q_0}{K_x - K_0} = \frac{rQ_m}{(1-a-\sqrt{1-r})K_m} = \frac{r(1-a)}{(1-a-\sqrt{1-r})} W_{01},$$
(3.9)

where r is the flow ratio between Q_x and Q_m, $Q_x = rQ_m$.

With the above equations, we have the relationship among W_{x0}, W_{x1} and W_{01}, which follows

$$W_{x1} = \frac{1}{2}(W_{x0} + W_{01}\sqrt{(\frac{W_{x0}}{W_{01}})^2 - 4(1-a)^2 \frac{W_{x0}}{W_{01}} + 4(1-a)^2}) .$$
(3.10)

By using a Taylor series expansion, W_{x1} can be approximated as

$$W_{x1} = \frac{1}{2}(aW_{x0} + 2(1-a)W_{01}) .$$
(3.11)

Back ward recovery shockwaves detection

When the signal changes to green, a backward recovery shockwave W_{01} is formed between stopped vehicles and the vehicles start to move forward. If the vehicle stopped

on the detection zone of vehicle detector starts to move after time; Let ΔT be the time difference between the time that green phase begins and the time that state of vehicle detector changes from stopped duration to moving duration (see Figure 3.7.). Following the concept proposed by May [16], the backward recovery shockwave can be calculated by,

$$W_{01} = -\frac{D}{\Delta T} \tag{3.12}$$

Where D is the distance from stop line to the location of detector.
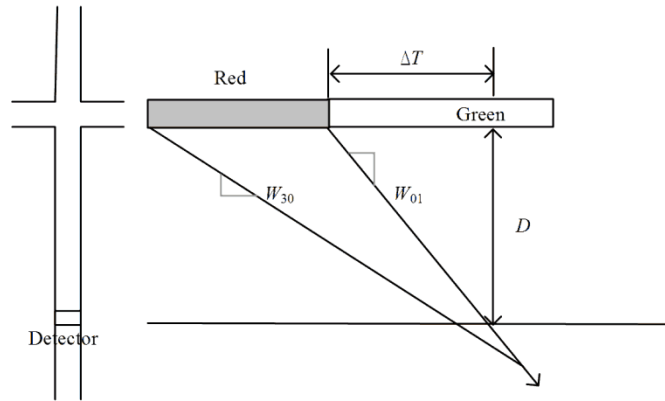
Figure 3.7 Backward recovery shockwave detection

Ideal forward recovery and backward forming shockwaves calculation

To calculate the shockwaves in an intersection, this study introduces two *ideal* shockwaves; one is the *ideal forward recovery shockwave*, the other is the *ideal backward shockwave*. The ideal forward recovery shockwave is formed at where the ideal arrival traffic flow that catches the forward moving saturation flow; the shockwave can be graphically shown as the boundary between state 2 and 1 in Figure 3.5.

The ideal flow rate, Q_2, can be calculated through green split of a signal cycle (g/c) and saturation flow rate (Q_m).

$$Q_2 = \frac{g}{c} Q_m = rQ_m \tag{3.13}$$

The flow ratio r between Q_2 and Q_m is equal to g/c. To replace x with 2 in Eq. (3.8), the ideal forward recovery shockwave can be calculated as,

$$W_{21} = (1-a)\sqrt{1-g/c} W_{01}. \tag{3.14}$$

Similarly, to replace x with 2 in Eq. (3.9), the ideal backward forming shockwave can be calculated as,

$$W_{20} = \frac{g/c(1-a)}{(1-a-\sqrt{1-g/c})} W_{01}. \tag{3.15}$$

The equations above show that the ideal shockwaves, W_{21} and W_{20}, can be simplified to a ratio of the backward recovery shockwave W_{01}. Therefore, with backward recovery shockwave W_{01}, green split and calibrated constant a, the ideal shockwaves can be calculated by Eq. (3.14) and (3.15).

Backward forming shockwaves detection

This subsection discusses the calculation of a backward forming shockwave. The calculation method can be categorized into two types: 1) the method which utilizes moving and empty duration, and 2) the calculation method which utilizes stopped duration. Parameters of moving duration and empty duration are generated from the detector while there are no stopped vehicles within the detection area; otherwise, the parameter of stopped duration is outputted.

Using moving duration and empty duration for general backward forming shockwave detection

Before the traffic queue reaches the detector, the sensor would output moving duration and empty duration. The relation among backward forming shockwave, moving duration and empty duration is illustrated in Figure 3.8.

As a vehicle i with speed V and length L_i passes a detecting zone with length L_z, this will result a moving duration m_i equal to $(L_i + L_z)/V$. As no vehicle within the detecting zone, it will result an empty duration e_i. Let E be the summation of all empty durations e_i and M be the summation of all moving duration m_i during a time interval ΔT. Assume the length of detecting zone be approximately the same as the gap between two stopped vehicles, then the summation of moving duration M can be calculated as the following equation,

$$M = \sum_{i=0}^{n} m_i = \sum_{i=0}^{n} \frac{(L_z + L_i)}{V} \approx \frac{L_q}{V} = \Delta t \, , \qquad (3.16)$$

where L_q denotes the queue length resulting from the vehicles during time interval ΔT, and Δt is the time interval shown in Figure 3.8. According the geometry relationship in Figure 3.8, the summation of all empty duration E can be calculated as

$$E = \Delta T - M \approx \Delta T - \Delta t \, . \qquad (3.17)$$

Moreover, the geometry relationship also leads to the following backward forming shockwave equation.

$$W_{30} = -\frac{L_q}{\Delta T - \Delta t} \approx -\frac{L_q}{E} = -\frac{MV}{E} \qquad\qquad (3.18)$$

The backward forming shockwave can be calculated using Eq. (3.18) with the parameters of vehicle speed (V), moving duration (M), and empty duration (E).
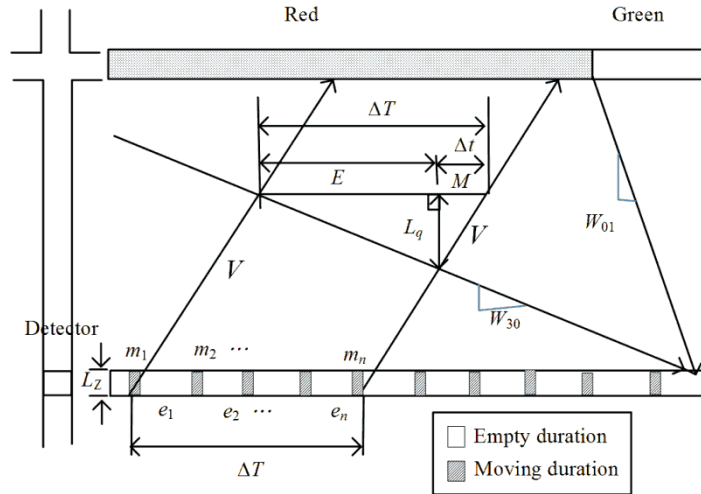
Fig. 3.8.   Relation among backward forming shockwave, moving duration and empty duration.

Using stopped duration for backward forming shockwave detection

After the queue reaches the detector during red phase, stopped duration would be used for shockwave calculation. Figure 3.9 and 3.10 illustrate the changes in the stopped duration for two consecutive signal cycles which have same red phase duration. Figure 3.9 demonstrates the case which the propagation speed of backward forming shockwave is greater than the ideal backward forming shockwave. It should be noted that since the propagation direction of backward forming shockwave is opposite to vehicle trajectory, the term *greater* actually means the absolute value of W_{30} is greater than the absolute value of W_{20}. In this case, the stopped duration is increasing for two consecutive cycles.

On the contrary, Figure 3.10 shows the case which the propagation speed of

backward forming shockwave is less than the ideal backward forming shockwave. The stopped duration in this case is decreasing for two consecutive cycles. Since the two cases resemble each other, the following analyses and equations can be applied to both cases.

Figure 3.9. Backward forming shockwave for $|W_{30}| > |W_{20}|$ (a) Shockwaves in flow-density diagram. (b) Shockwave and incremental stopped duration. (c)Incremental stopped duration in red phase. (d) Incremental stopped duration in green phase.

The stopped duration of the first cycle is $\overline{O_1A_1}$, while that of the second cycle is $\overline{O_2C_2}$. $\overline{O_1A_1}$ is almost equal to $\overline{O_2A_2}$ if the traffic flow changes smoothly. Hence, the stopped duration difference for these two consecutive cycles is $\overline{A_2C_2}$, or ΔS_C. Since the dashed lines have the same slope as the shockwave W_{30}, $\overline{AC}$ is equal to $\overline{A_2C_2}$. $\overline{AC}$ is the sum of $\overline{AB}$ and $\overline{BC}$. $\overline{AB}$ has the same length as ΔS_R and $\overline{BC}$ has the same length as ΔS_G. $\overline{BC}$, or ΔS_G, is derived from the flow difference between shockwaves W_{21} and W_{31} during the green phase G. $\overline{AB}$, or ΔS_R, can be calculated from the flow difference between shockwaves W_{20} and W_{30} during the red phase R.

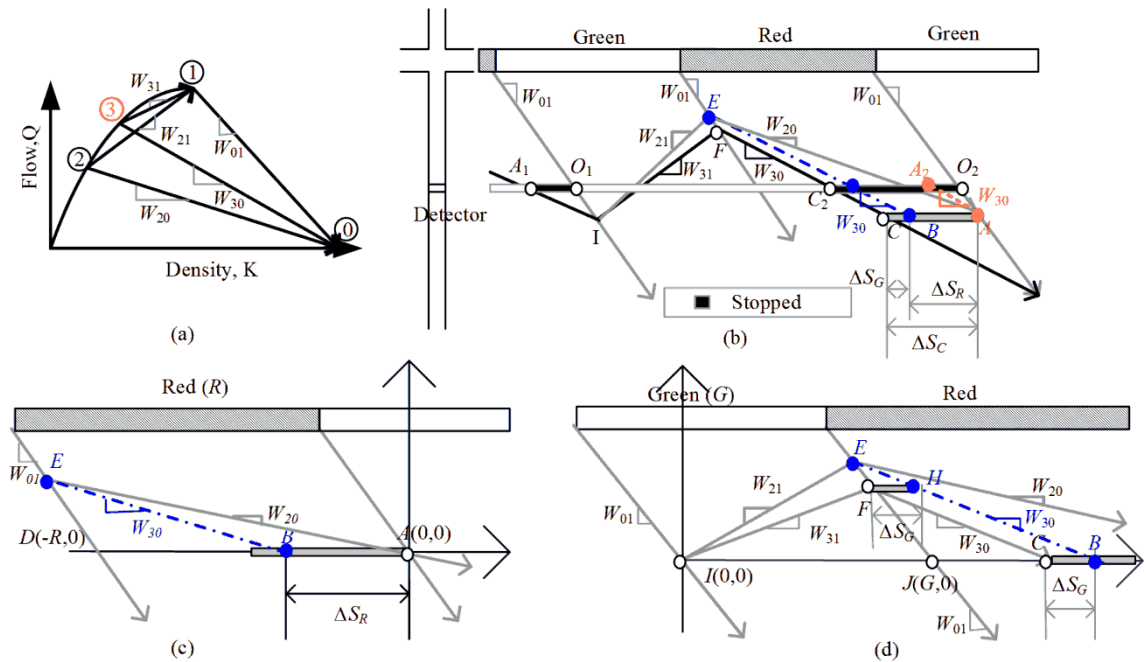Figure 3.10. Case for backward forming shockwave $|W_{30}| < |W_{20}|$ (a) Shockwaves in flow-density diagram. (b) Shockwave and reductive stopped duration. (c) Reductive stopped duration in red phase. (d) Reductive stopped duration in green phase.

Therefore,

$$\Delta S_C = \Delta S_G + \Delta S_R \tag{3.19}$$

To calculate ΔS_R, we should consider Figure 3.9(b) and Figure 3.9(c). Let a Euclidean space represents the time-space diagram of Figure 3.9(c) and set point A to be $(0, 0)$. In this case, the shockwave propagation speed, W, is acted as slope. By using linear algebra, point E can be obtained from lines AE and DE,

$$E(X_E, Y_E): \begin{cases} \overleftrightarrow{AE} : Y = W_{20}X \\ \overleftrightarrow{DE} : Y = W_{01}(X + R) \end{cases} \tag{3.20}$$

Furthermore, point B can be derived from lines AB and BE,

$$B(\frac{RW_{01}(W_{20}-W_{30})}{W_{30}(W_{01}-W_{20})},0):\begin{cases}\overleftrightarrow{AB}:Y=0\\\overleftrightarrow{BE}:Y-Y_E=W_{30}(X-X_E)\end{cases} \tag{3.21}$$

Hence

$$\Delta S_R = \overline{AB} = \frac{RW_{01}(W_{20}-W_{30})}{W_{30}(W_{01}-W_{20})} \tag{3.22}$$

Similarly, ΔS_G can be calculated from the flow difference between shockwave W_{21} and W_{31} during the green phase G. To calculate $\Delta 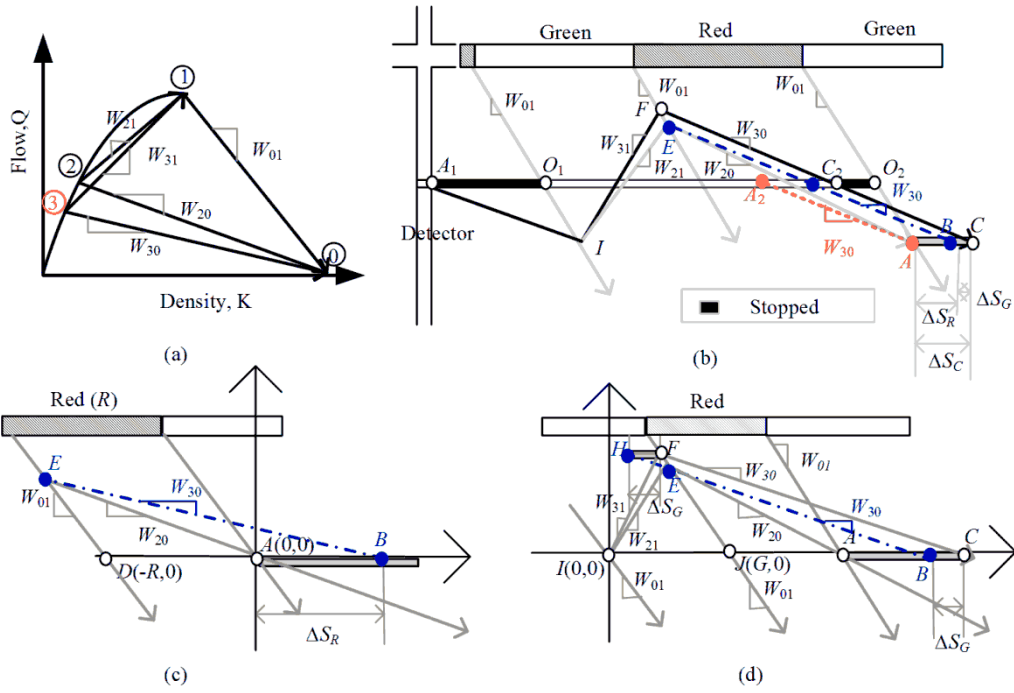S_G$, we should consider Figure 3.9(b) and Figure 3.9(d). Let a Euclidean space represents the time-space diagram of Figure 3.9(d) and set point I to be (0, 0). The point E can then be obtained from lines IE and JE using linear algebra

$$E(\frac{GW_{01}}{W_{01}-W_{21}},\frac{GW_{01}W_{21}}{W_{01}-W_{21}}):\begin{cases}\overleftrightarrow{IE}:Y=W_{21}X\\\overleftrightarrow{JE}:Y=W_{01}(X-G)\end{cases} \tag{3.23}$$

Also point F can be derived from lines IF and JF,

$$F(\frac{GW_{01}}{W_{01}-W_{31}},\frac{GW_{01}W_{31}}{W_{01}-W_{31}}):\begin{cases}\overleftrightarrow{IF}:Y=W_{31}X\\\overleftrightarrow{JF}:Y=W_{01}(X-G)\end{cases} \tag{3.24}$$

And point H can be calculated from lines FH and EH,

$$H(X_H, Y_H) : \begin{cases} \overrightarrow{FH} : Y = Y_F \\ \overleftarrow{EH} : Y - Y_E = W_{30}(X - X_E) \end{cases} \tag{3.25}$$

Therefore

$$\Delta S_G = \overline{BC} = \overline{FH} = \frac{GW_{01}(W_{01} - W_{30})(W_{31} - W_{21})}{W_{30}(W_{01} - W_{21})(W_{01} - W_{31})} \tag{3.26}$$

Replace x by 3 in equation (3.11), we would have the following equation,

$$W_{31} = \frac{1}{2}(aW_{30} + 2(1-a)W_{01}) \tag{3.27}$$

Substitute W_{21} and W_{31} in equation (3.26) by equation (3.14) and (3.27),

$$\Delta S_G = \frac{GW_{01}(W_{01} - W_{30})(W_{30} - W_{20})}{W_{30}(W_{01} - W_{21})(2W_{01} - W_{30})} \tag{3.28}$$

Therefore, ΔS_C can be calculated by

$$\Delta S_C = \Delta S_G + \Delta S_R = \frac{GW_{01}(W_{01} - W_{30})(W_{30} - W_{20})}{W_{30}(W_{01} - W_{21})(2W_{01} - W_{30})} + \frac{RW_{01}(W_{20} - W_{30})}{W_{30}(W_{01} - W_{20})} \tag{3.29}$$

The calculation of shockwaves with parameter of stopped duration, the following procedure can be applied. We have the red phase duration R and green phase duration G

given by traffic controller; and the backward recovery shockwave W_{01} calculated by Eq. (3.12). When there is no spillover, the speed of shockwave W_{01} is nearly constant. The ideal shockwaves, W_{20} and W_{21}, can be calculated from Eq. (3.14) and (3.15) with given R and G. Therefore, the stopped duration differences, ΔS_C, can immediately be calculated after detecting a stopped vehicle. After deriving stopped duration difference, from vehicle detection, the backward forming shockwave W_{30} can be calculated by Eq. (3.29).The calculating procedure can be applied to Figure 3.10 and having the same result.

If the red phase duration (R) is not fixed for two consecutive cycles, then Eq. (3.29) must be modified as,

$$\Delta S_C = \Delta S_G + \Delta S_R + \Delta R = \frac{GW_{10}(W_{10}-W_{30})(W_{30}-W_{20})}{W_{30}(W_{10}-W_{21})(2W_{10}-W_{30})} + \frac{RW_{10}(W_{20}-W_{30})}{W_{30}(W_{10}-W_{20})} + \Delta R \qquad (3.30)$$

where ΔR is the red phase duration difference of two consecutive cycles.

Backward forming shockwave detection under heavy congestion

If the queue has the length more than the vehicle detector installation location plus the length of queue that can be discharged during green phase, it would cause the detector to output the traffic parameter of stopped duration be the same as red phase duration, as Figure 3.11. In this case, Eq. (3.29) and (3.30) cannot be used to calculate the backward forming shockwave. Additional vehicle detectors can be added to solve this problem; the Eq. (3.29) and (3.30) can be applied to new detectors. If the installation of new detector is not possible, the moving average, as Eq. (3.31), can be used to predict the backward forming shockwave.

$$W_{30}(n) = \frac{1}{5}W_{30}(n-1) + \frac{1}{5}W_{30}(n-2) + \frac{1}{5}W_{30}(n-3) + \frac{1}{5}W_{30}(n-4) + \frac{1}{5}W_{30}(n-5) \quad (3.31)$$

where $W_{30}(n)$ is current shockwave value, $W_{30}(n-i)$ is the *i-th* previous shockwave value.
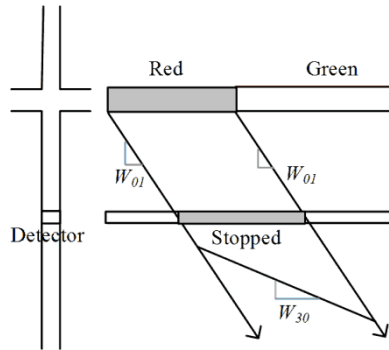
Figure 3.11 A vehicle's stopped duration is equal to the red phase time.

Forward recovery shockwave detection

The forward recovery shockwave can easily be calculated using Eq. (3.27). The backward recovery shockwave W_{01} is calculated first, followed by the backward forming shockwave W_{30}. The forward recovery shockwave, W_{31}, is the last shockwave to be calculated. The sequence of shockwave estimation determines the model's prediction capability. Liu and Wu [29, 17, 30] could not provide any predictions because their models had computed the forward recovery shockwave before the backward forming shockwave. In this study, three shockwaves can be derived right after the detection of stopped vehicle and much traffic information can be predicted. Compare to existing researches, which the shockwaves can only be derived after the beginning of green time; the proposed method can predict shockwaves earlier and supports an adaptive traffic control model more efficiency.

Shockwaves detection algorithm

This subsection proposes an algorithm to calculate shockwaves that being

discussed in the previous subsections. The proposed algorithm is demonstrated as figure 3.12(a). First, gather presence data from vehicle detector; second, calculate traffic parameters including empty duration, moving duration, and stopped duration. Third, the calculation of backward recovery shockwave and followed by fourth, the calculation of ideal shockwaves. Fifth, backward forming shockwave is calculated. Last, forward recovery shockwave is obtained. The estimation method of backward forming shockwave is detailed in Figure 3.12(b). This figure demonstrates the usage of multiple detectors to predict backward forming shockwave; although the figure illustrates the procedure by two detectors, it can be easily extended to multiple detectors. The first step is setting a vehicle detector near the stop line and the other at the upstream. The spacing between detectors should be more than the length of queue that can be discharged during maximal green time. If the first detector do not gives a stopped duration, then the moving duration and empty duration of first detector is utilized in the calculation of backward forming shockwave. Otherwise, stopped duration is taken into consideration. Moreover, if the stopped duration is larger than red time, the next detector should be considered; the above procedure should be repeated again for the next detector. The whole procedure ends at the last detector. If all detectors have the stopped durations as red time, estimation method of Eq. (3.31) should be used.

3.4 Upstream speed and flow detection

This sub-section focuses on the estimation of upstream speed and flow. The upstream means the state which is not affected by the queue; state 3 is a common representative.

After deriving W_{x0}, W_{x1} and W_{01} (Eq. 3.7-3.11), the flow ratio r between Q_x and Q_m can be calculated as

$$r = \frac{W_{x0}\sqrt{4(a-1)^2W_{01}^2 - 4(a-1)^2W_{01}W_{x0} + W_{x0}^2} + 2(a-1)^2W_{01}W_{x0} - W_{x0}^2}{2(a-1)^2W_{01}^2} .$$ (3.32)
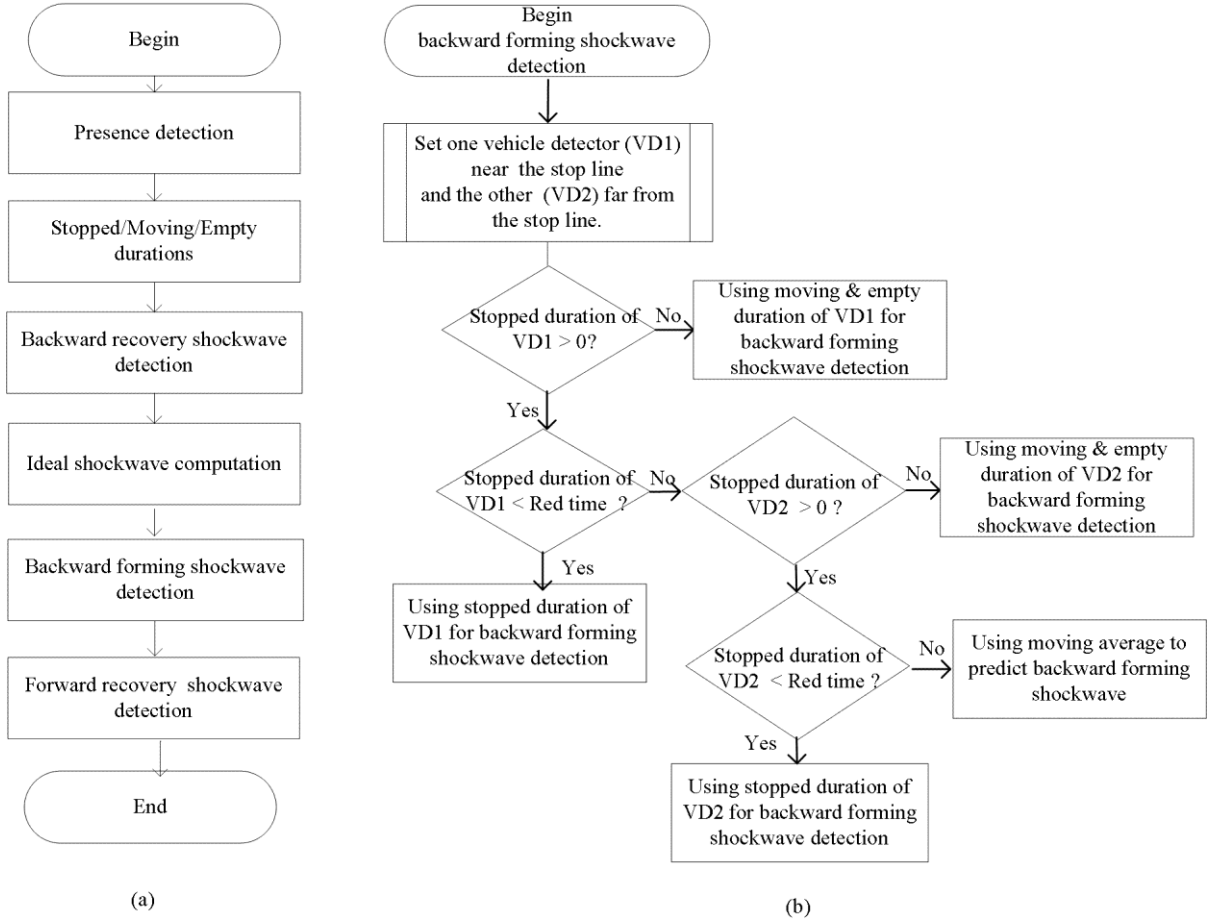

Figure 3.12 (a) The flowchart for five shockwaves detection. (b) The flowchart for backward forming shockwave detection.

Therefore, the corresponding space mean speed U_x and flow rate Q_x can be calculated as

$$U_x = \frac{(1-a)r}{1-\sqrt{1-r}}W_{01}$$ (3.33)

$$Q_x = \frac{W_{x0}\sqrt{4(a-1)^2W_{01}^2 - 4(a-1)^2W_{01}W_{x0} + W_{x0}^2} + 2(a-1)^2W_{01}W_{x0} - W_{x0}^2}{2(a-1)^2W_{01}^2}Q_m \qquad (3.34)$$

If all shockwaves of state 3 are derived, the arrival flow rate can be calculated by Eq. (3.34). Replace x with 3 in Eq. (3.32), the arrival flow ratio r is

$$r = \frac{W_{30}\sqrt{4(a-1)^2W_{01}^2 - 4(a-1)^2W_{01}W_{30} + W_{30}^2} + 2(a-1)^2W_{01}W_{30} - W_{30}^2}{2(a-1)^2W_{01}^2} \qquad (3.35)$$

The flow is calculated as the following equation,

$$Q_3 = rQ_m = \frac{W_{30}\sqrt{4(a-1)^2W_{01}^2 - 4(a-1)^2W_{01}W_{30} + W_{30}^2} + 2(a-1)^2W_{01}W_{30} - W_{30}^2}{2(a-1)^2W_{01}^2}Q_m \qquad (3.36)$$

where Q_m is the saturation flow rate, which can be investigated–in advance. The speed of state 3 can be derived from Eq. (3.33),

$$U_3 = \frac{(1-a)r}{1-\sqrt{1-r}}W_{01} \qquad (3.37)$$

where U_3 represents the space mean speed of state 3.

3.5 Signal control algorithm

This section comprises three parts: 1) the critical paths of closely spaced intersections, 2) the design of phase sequence for path-based progression, and 3) the improvement of full-actuated control by which prevents capacity loss.

Critical paths of closely spaced intersections

A critical path of closely spaced intersections is defined as a major demand path

of origin-destination flows. With the intersections being closely spaced, the origin-destination can be easily observed at the field side. Figure 3.13 gives an example of closely spaced intersections with four critical paths.

Stop line is essential in the computation of shockwaves. To evaluate the progression of a path, shockwaves of a path is introduced instead of shockwaves of an approach. Therefore, an important concept is introduced here, the stop line of a critical path. The stop line of a critical path is defined as the first stop line that one would encounter along with the critical path. In Figure 3.13, the stop line of each path is denoted as a thick black bar.

Phase sequences for critical paths

Most closely spaced intersections can benefit from signal progression, which avoids unnecessary stops and delays. The design of one- or two-way progression usually relays on a time-space diagram, which graphically illustrates how traffic propagates through intersections. The bandwidth of a time-space diagram is the portion of cycle which allows vehicle to go through all intersections in a group without stopping. Figure 3.14(a) demonstrates a typical time-space diagram which contains a one-way bandwidth; the bandwidth allows vehicles to traverse through 3 intersections without stopping. However, designing phase sequences for closely spaced intersections may depend on path-based progression that cannot be analyzed easily by traditional time-space diagram.

From a signal timing perspective, phase sequence determines the quality of progression at signalized closely spaced intersections. Therefore, if one desires to conduct a multi-path progression, phase sequence must be designed carefully for vehicles along each critical path. We propose a new path-based progression method

that use path-intersection diagram to design phase sequence. Figure 3.14(b) shows the designed phase sequences for each critical path corresponding to Figure 3.13. By the path-intersection diagram, one can easily arrange the phase sequences along each critical path.
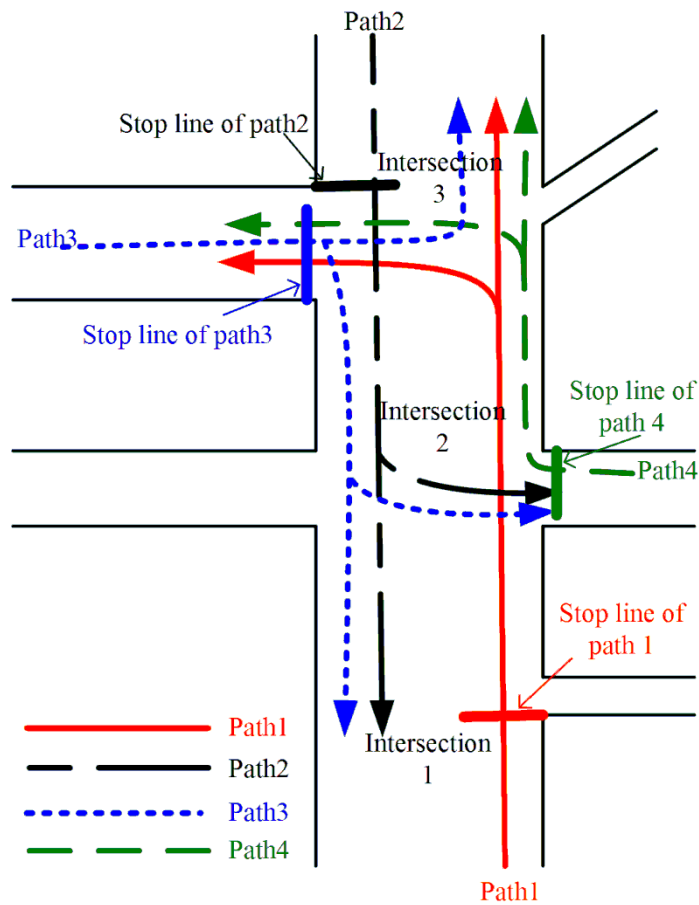
Figure 3.13 Four critical paths in three closely spaced intersections

Path-based progressions are guaranteed by providing dedicate phases for each critical path. After designing phases for critical paths, phases on minor paths are arranged correspondingly in a manner that avoids conflict points on critical paths. The path-intersection diagram provides actuated control capabilities through their ability to respond to cycle-by-cycle variation in traffic demand while still being able to provide

progression for critical path movement.
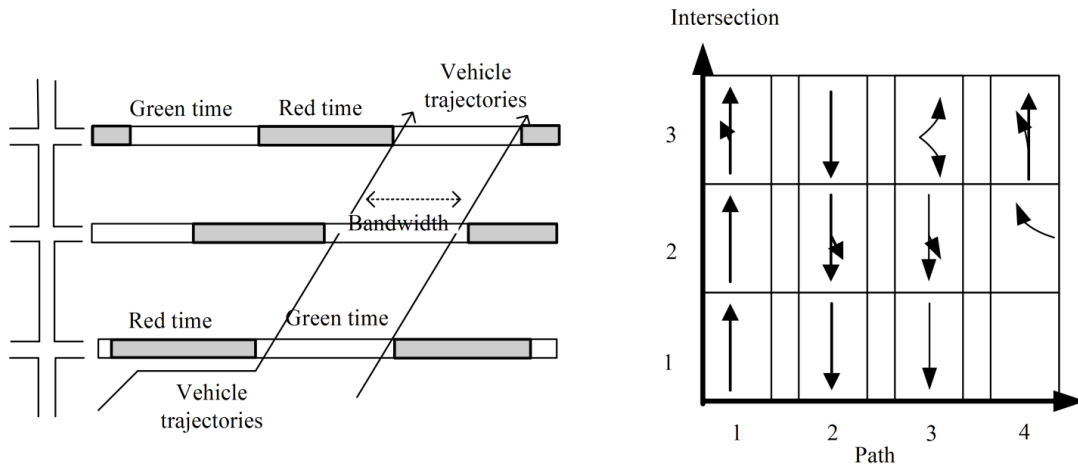
Figure 3.14 (a)A one-way progression in time-space diagram.   (b) A four-way progression in path-intersection diagram. The phase sequences are corresponding to Figure 3.13.

Enhanced actuated control

A full-actuated traffic control uses both detector information and a set of control parameters to operate the intersection in an efficient way. The full-actuated controller allocates green times for each approach corresponding to traffic demands. Little traffic demand on an approach would results a shorter green time which provides fast turnovers to serve other approaches.

As shown in Figure 3.15(a), the minimum green time is allocated to a phase once a detector associated with that phase is actuated by a vehicle. If vehicles continue to actuate the detector while the phase is green, an additional green time equal to the vehicle extension time is added to the phase. The green can be extended until it reaches the maximum green at which time the phase terminates in a condition called a "Max Out." However, if no detector is actuated within a vehicle extension period (gap threshold), the phase is terminated in a condition called a "Gap Out."

A defect of full-actuated control can be observed in Figure 3.15(b). If a vehicle stops on detection zone, the vehicle will continue to actuate the detector until "Max out". However, under stop-and-go condition, vehicles often stop on the detector until "Max out". Although green time is allocated for the congested approach, no vehicles can be served. This prohibits the opportunity for traffics on different approaches to make use of the reserved capacity on intersection, and results a capacity loss.

(a)   (b)
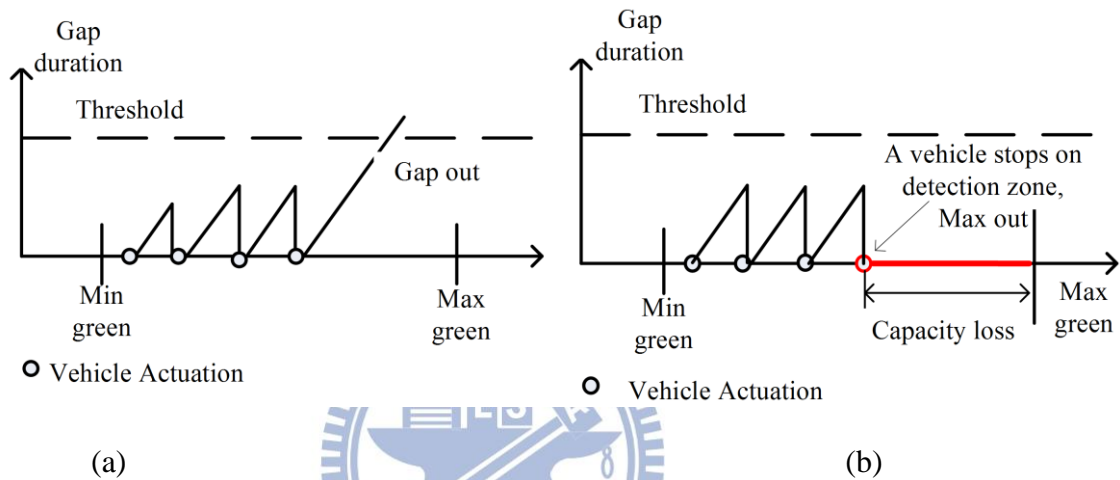
Figure 3.15 Full-actuated control with (a) gap out. (b)max out when a vehicle stops on detection zone.

To improve the defect, this research utilizes three new parameters to provide an enhanced actuated control operation (see Figure 3.16). The empty duration has a same physical meaning as gap duration, the axis "Gap duration" can be replaced by "Empty duration" in full-actuated control. A new parameter, Stopped duration, is introduced to overcome the problem of inefficient "Max out" problem. As a vehicle stops on the detection zone for an extensive time, a termination of current phase will be conducted as "Stopped out." This provides the opportunity for traffics on other approaches to be served. The concept of "Stopped out" is illustrated by new axis "Stopped duration" in Figure 3.16(b).
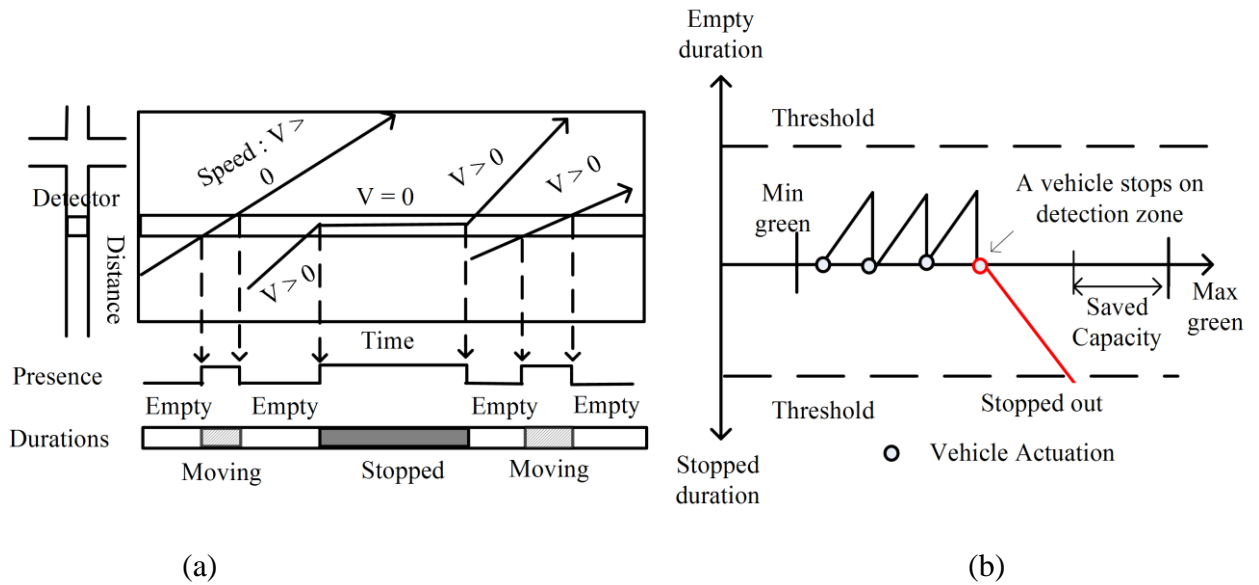
Figure 3.16 (a) Three traffic parameters: empty, moving and stopped durations. (b) Enhanced actuated control with a "stopped out" condition.

Dynamic green time model

With the above enhanced actuated control, we can construct the following model to optimize green times for closely spaced intersections. The key concepts include detecting the path shockwaves, dynamic green time formulation and optimize the path green time.

This subsection combines the vehicle stopped duration and shockwave theory to estimate the required green time of each critical path. The required green time will be dynamic adjusted according the critical path traffic demands. As shown in Figure 3.17, let point O be the origin of a Euclidean space, S be the duration that a vehicle stops on the detection zone, d be the distance from path stop line to detection zone and t_1 be the begin time of a vehicle which stops on the detection zone. Using the "point-slope" form for straight-line equations, the line AC, line BC and point C can be calculated as

$$C(\frac{W_{10}t_2 - W_{30}t_1}{W_{10} - W_{30}}, \frac{W_{30}W_{10}S}{W_{10} - W_{30}} + d) : \begin{cases} \overleftrightarrow{AC} : y - d = W_{30}(x - t_1) \\ \overleftrightarrow{BC} : y - d = W_{10}(x - t_2) \end{cases} \tag{3.38}$$

Similarly, if traffic follows the Greenshields model, the line CE, line OE and point E can be calculated as

$$E(\frac{SW_{10}^2}{(W_{10} - W_{30})^2} + \frac{d}{W_{10} - W_{30}} + t_1, 0) : \begin{cases} \overleftrightarrow{CE} : y - \frac{W_{30}W_{10}S}{W_{10} - W_{30}} - d = W_{31}(x - \frac{W_{10}t_2 - W_{30}t_1}{W_{10} - W_{30}}) \\ \overleftrightarrow{OE} : y = 0 \end{cases} \tag{3.39}$$

Hence, the required green time g (line segment OE) is calculated as:

$$g = \frac{SW_{10}^2}{(W_{10} - W_{30})^2} + \frac{d}{W_{10} - W_{30}} + t_1 \tag{3.40}$$

That is to say, required green time can be known after shockwaves and stopped durations have been detected.
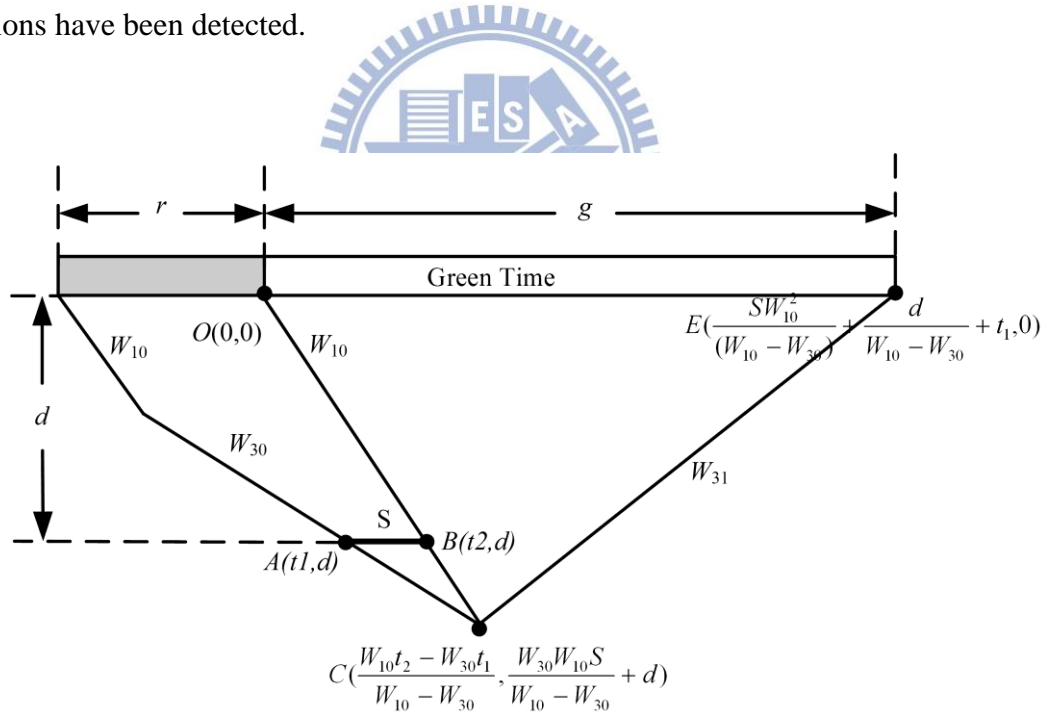

Figure 3.17 The relation between required green time and shockwaves.

Green time optimization model

With the above dynamic green time formulation, we can construct the following model to optimize green timings along all critical paths.

Under unstable condition, unbalanced green time may lead to a longer congestion

time than balanced green time. With different demand on paths, the overall congestion time can be minimal if the green time for each path is proportion to its corresponding traffic demand. If the green times of different paths were not proportion to its demand, some demands would have a longer congestion time compare to others. Therefore, the objective of green time optimization model becomes determine the optimal green time for each path. The optimal green time can be derived by balancing out the traffic demands on all paths. Balanced path green times also ensures less total delay time and short travel time [19].   The optimized green times are modeled as following equations.

$$\text{Min} \left| \frac{G_1}{G} - \frac{g_1}{g} \right| + \left| \frac{G_2}{G} - \frac{g_2}{g} \right| + ... + \left| \frac{G_n}{G} - \frac{g_n}{g} \right| \tag{3.41}$$

Such that

$$g = g_1 + g_2 + g_3 + ... + g_n \tag{3.42}$$

$$G = G_1 + G_2 + G_3 + ... + G_n \tag{3.43}$$

$$G = \max(G_{min}, \min(g, G_{max})) \tag{3.44}$$

$$G_{i,min} \leqq G_i \leqq G_{i,max} \quad , 1 \leqq i \leqq n \tag{3.45}$$

where g_i is the required green time for path i to discharge its traffic demand (which is calculated by Eq. 3.40); G_i is optimized green time for path i; G_{max} and G_{min} are the maximal and minimal value for the summation of optimized green times, respectively; $G_{i,min}$ and $G_{i,max}$ are the lower and upper bound of green time for each critical path i, respectively. Eqs. (3.43)-(3.44) restrict the summation of optimized green time between maximal and minimal value. Eq. (3.45) requires that the green time for each path should satisfy its lower bound, but not exceed its upper bound.
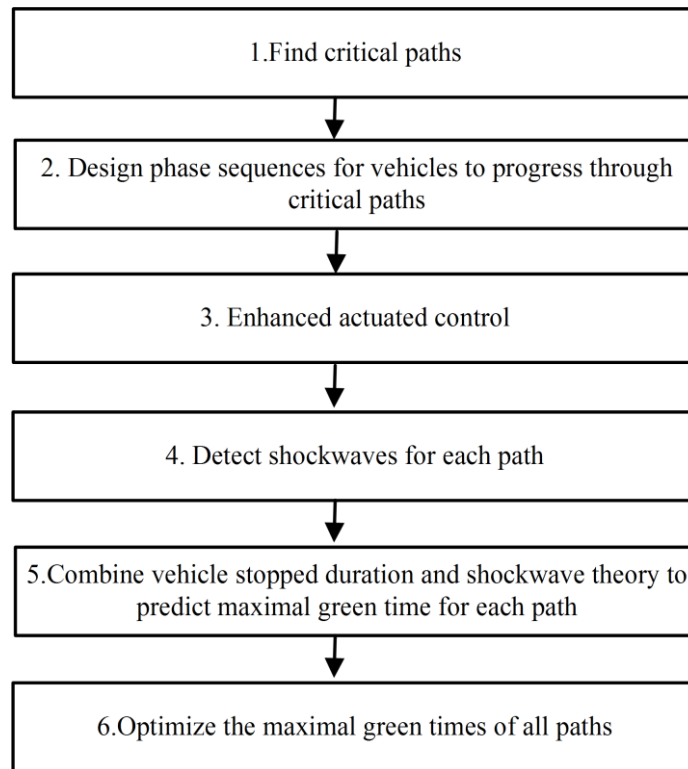
Figure 3.18   Flowchart of actuated critical path control algorithm.

Control algorithm

The flowchart of the proposed algorithm is illustrated in Figure 3.18, there are six

steps to form the critical path control method. The first 3 steps are focused on planning

side; while the last 3 steps execute in the traffic signal controller. The first step finds the

critical paths for closely spaced intersections. At the field side, one can collect traffic

flow data to figure out the major origin-destination paths. The second step focused on

designing phase sequences for multiple path-based progressions. The phase sequence is

designed by the path-intersection diagram. Each path has a dedicated phase to progress

the path movement. After phasing, the enhanced actuated control should be employed to

prevent capacity loss.   During the operation of actuated control, step four detects path

shockwaves,   including   backward   forming   shockwave   and   backward   recovery

shockwave. Step five predicts the required green time for each path by Eq. (3.40). The begin time and duration for a vehicle stopped on detection zone should be collected at this step. During the last step, required green times are optimized for all paths. The enhanced actuated control utilizes the optimized green time as the maximal green time for each critical path.
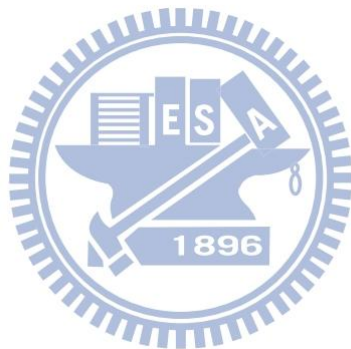
IV. Results and Discussion

In this chapter, the proposed models are tested with real networks to discuss their performance. These models include i) radar vehicle detection method in section 4.1 ii)three new traffic parameters in section 4.2 iii)shockwaves detection in section 4.3 iv)upstream flow and speed detection in section 4.4 and v) traffic signal control algorithm in section 4.5.

4.1 Radar vehicle detector

In this section, the radar system is first introduced and the requirements of radar sensor are also presented. The algorithm of vehicle classification and speed estimation will be shown in following subsections.

Table 4.1   The specifications of radar sensor.

Height	4 - 7 m
Central frequency	10.5 G Hz
Band width	50 M Hz
Pulse repeat frequency	1500 Hz
Down range resolution	3 m
Max Range	60 m
Max range shift frequency	30 K Hz
Elevation angle/Azimuth angle	50 ° / 20 °
ADC	200 K Hz
FFT	128 points

Radar system

To support multi-lane capabilities, the FMCW radar detector is designed for roadside installation, as illustrated in Figure 4.1(a). The sensor is installed at a height of 5.2 meters above the ground and at a distance of 14 meters from the first lane. The maximal distance is 32 meters of the sensor from the most distant lane. The echo power of each lane is near-constant from the distance 14 to 32 meters. The dashed line is a curve that fits the echo power distribution of the vehicle on the road surface. The central frequency is 10.5 GHz. The vehicle width leads the radar with 50 M Hz band width and 3 meters down range resolution. The radar is designed to cover a maximum of eight lanes, and can be positioned a maximum of 60 meters from the roadside. The total frames per second, or the pulse repeat frequency, are 1500 Hz. Therefore, the max range shift frequency is 30 K Hz. The corresponding radar signal processing speed for ADC is 200 K Hz. Furthermore, the elevation and azimuth angles of the planar antenna are 50° and 20°. The specifications of the radar system are summarized in Table 4.1.
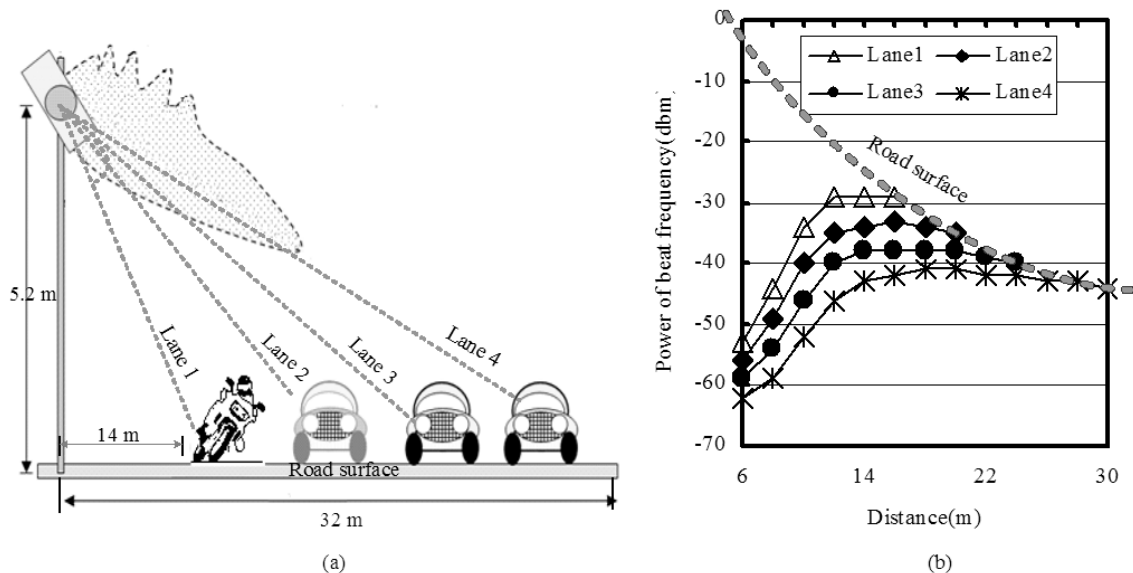

Figure 4.1 (a) Installation of radar sensor. There are four lanes. (b)The echo powers distribution for each lane of road.
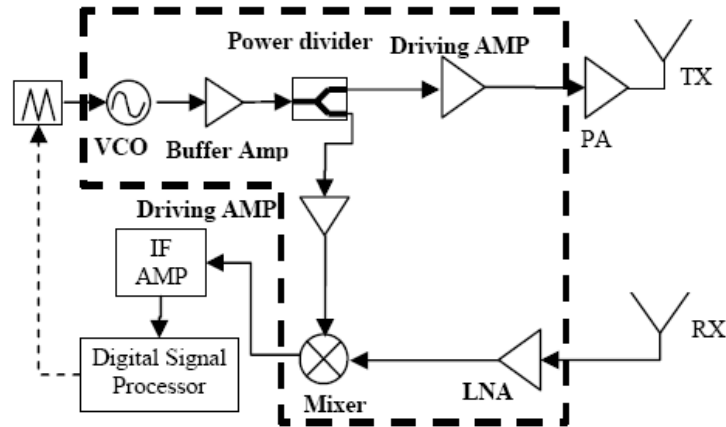
Figure 4.2. Block diagram of the proposed X-band FMCW sensor system.

The building blocks of the X-Band FMCW of the radar are shown in Figure 4.2. The sensor comprise two external antenna arrays, a single-chip CMOS transceiver (enclosed by the dashed line) and an external digital signal processing unit along with the necessary electronics. A power amplifier is added to increase output power level. Dual planar antenna array are located at the transmitter output and the receiver input. The planar antennas have an equivalent STC function. As shown inside the dashed lines, the radio frequency transceiver is a chip based on a standard 0.18 μm CMOS technology [45, 46]. The CMOS transceiver performs most of the required RF signal processing. A power amplifier is added to increase output power. Furthermore, a baseband digital signal processing unit is used for instantaneous and simultaneous assessment of range measurements. Figure 4.1(b) illustrates the beat frequency power distribution of the antenna corresponding to the installation in Figure 4.1(a).   There are four echo power curves for four lanes. Generally, the echo power of most antennas decays at a rate $1/R^4$. For this specially designed planar antenna, the shorter range power decay can be cancelled by the near field interference. The dashed line, shown in

Figure 4.1(b), is the road surface curve. Restated, the echo power of the vehicle signal will stay on the four inter-points of the road surface curve. The empirical results, illustrated later in this section, show that complementing the magnitude of the vehicles with the second power of the frequency can obtain an accurate vehicle classification rate.

Vehicle classifier and speed estimation

Table 4.2 lists a data set to train two classifiers : SVM and LDA. The data had been collected on the Hsin-Lon road of the Chu-Pei city. Generally, users require installing the radar sensor as soon as possible. During the short setup time, the numbers of vehicle in four categories is skew. A good classifier requires an acceptable classification rate, after applying its learning algorithm to skew data constraints. The training data satisfies the short setup time and skew data constraints.
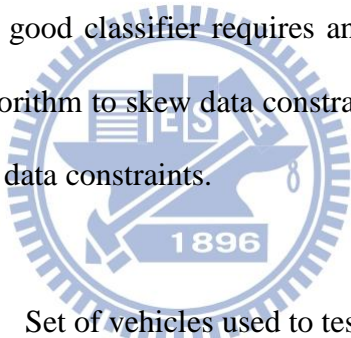
Table 4.2   Set of vehicles used to test the classifiers.

	Motorcycle	Small	Medium	Large
Total	30	145	12	4

After applying the K-means, LDA and SVM to the training data in Table 4.2, the classification rate is 42%, 93% and 94%, respectively. In Table 4.3, the rate results in K-means not being a good classifier in situations involving constraints. The LDA and SVM have a near identical leave-one-out recognition rate, and moreover this rate is acceptable. Both methods are good classifiers, and can resolve any associated environmental installation problems. The following paragraphs analyze and compares these two classifiers more details.

Table 4.3   The classification rate of classifiers.

K-means	LDA	SVM
42%	93%	94%

Table 4.4 Vehicles obtained from a field.

Category	Motorcycle	Small		Medium	Large
Type ID	1	2	3	4	5
Type	motorcycle	Car	van	Bus	Truck
Subtotal	30	79	66	12	4
Total	191				

Table 4.4 lists another testing data set that meets the short setup time and skew data constraints. The test data were obtained from a field site on a road in Chu-Pei city, Taiwan. The radar is installed as illustrated in Figure 3.1. The same traffic volume can be collected on a normal urban road within a 10-15 minutes period. The five vehicle types from the table can be classified into four categories. All vehicles from different lanes are merged into a single training data set. According to the radar equation, in Eq. (4.1), the receiver power of the vehicle is decayed by $1/R^4$. As shown in Figure. 4.1(b), the planar antenna is specially designed to perform an SPC function which compensates for the decay in each lane. The receiver power of the road surface, indicated by the dashed line curve, resembles a curve with some power of the range. Therefore some software STC functions are tested, as shown in Eq. (3.3), to compensate for the decay of the road surface.   Before extracting the features from the vehicle profile, amplitude of

71

the profile is multiplied by some power of the frequency. Although the classifier is designed to classify vehicles into four categories, recognition rates remain an area of interest for numerous combinations of different vehicle types.

$$P_r = \frac{P_t G^2 \lambda^2 \sigma}{(4\pi)^3 R^4},$$ (4.1)

where P_r denotes receiver power, P_t represents transmitter power, λ is wave length, G denotes antenna gains, σ represents RCS, and R is vehicle range.

Table 4.5. Leave-one-out recognition rate for different classifiers and categories.

Category	LDA(f_m)	SVM(f_m)	LDA(f_m^2)	SVM(f_m^2)	LDA(f_m^4)	SVM(f_m^4)
1 vs. 2 vs. 3 vs. 4 vs. 5	73%(140/191)	76%(145/191)	76%(146/191)	82%(156/191)	78%(149/191)	71%(136/191)
1 vs. 2345	95%(182/191)	98%(187/191)	96%(183/191)	99%(189/191)	94%(180/191)	97%(186/191)
1 vs. 23 vs. 4 vs. 5	93%(177/191)	94%(180/191)	95%(181/191)	98%(186/191)	93%(178/191)	93%(177/191)
23 vs.45	96%(155/161)	97%(156/161)	97%(156/161)	99%(159/161)	96%(154/16)	96%(155/161)
23 vs. 4 vs. 5	96%(155/161)	96%(155/161)	98%(158/161)	98%(158/161)	96%(154/161)	95%(153/161)
2 vs. 3 vs. 4 vs. 5	72%(116/161)	75%(121/161)	75%(121/161)	80%(128/161)	76%(123/161)	71%(115/161)
2 vs. 3	76%(110/145)	75%(109/145)	77%(112/145)	79%(114/145)	78%(113/145)	74%(108/145)
4 vs. 5	88%(14/16)	94%(15/16)	88%(14/16)	94%(15/16)	94%(15/16)	100%(16/16)

Table 4.5 lists the test results for different powers of frequency for SVM and LDA. The highlighted cells represent the highest leave-one-all recognition rates for different categories. SVM wins almost all scenarios in f_m^2 cases. Table 4.6 lists the error matrix for a SVM(f_m^2) case. Therefore, by compensating the received radar signal with power two of the frequency, SVM can obtain the best recognition rate. The first row ," 1 vs. 2 vs. 3 vs. 4 vs. 5" , indicates a low recognition rate for each classifier. This low rate means that creating excessively narrow categories will result in a low recognition rate. Comparing the third and fifth rows, "1 vs. 23 vs. 4 vs. 5" and "23 vs. 4 vs. 5", reveals that the recognition rates are almost equal in the same classifier. Motorcycles can

generally be separated from other vehicle types. The second row, "1 vs. 2345", confirms this. Examining the last two rows, "2 vs. 3" and "4 vs. 5", reveals that car and van are difficult to separate, while bus and truck can generally be separated.

Table 4.6.   Leave-one-out error matrix for SVM($f_m{}^2$) .

Detect vehicle class	Actual vehicle class			
	Motorcycle	Small	Medium	Large
Motorcycle(1)	29	1	0	0
Small(2,3)	1	143	1	0
Medium(4)	0	1	11	1
Large(5)	0	0	0	3
Total	30	145	12	4
error (%)	3%	1%	8%	25
Recognition rate (%)	98%			

Table 4.7 shows the calibrated virtual loop length which is outputted from the video calibrating system. The far lane is slightly longer than the near lane. The planar antenna design is responsible for this effect. Figure 4.3 shows the vehicle length outputted by SVR. The estimated truck lengths are shorter than the visually measured lengths obtained from the video system, and the estimated motorcycle lengths are longer than the visually measured ones (see Figure 4.3 (b)).   The reason is that total number of vans and cars is 75%. The training data is skew, leading SVR make length predictions for all vehicles that are close to those of cars. Figure 4.4 describes the vehicle speed. Since the estimates of motorcycle length are high, the motorcycle speed always exceeds that of visual measurements obtained using the video system (see Figure 4.4(b)). The situation for trucks is the reverse of the above, with estimates of length and speed being lower than the visual measurements.
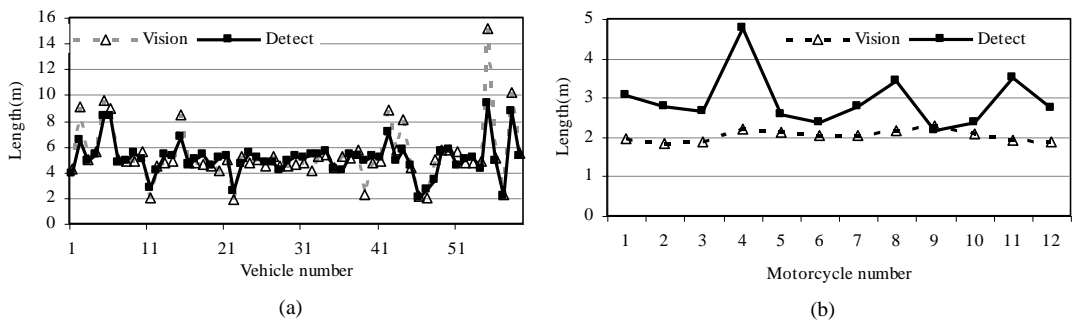
(a)   (b)

Figure 4.3. Vehicle output lengths from SVR. The open triangles with dashed lines denote the lengths measured from the video calibrating system. Meanwhile, the rectangles with black lines represent the estimated lengths obtained using the proposed algorithm. (a) The vehicle lengths were outputted from SVR. (b) The motorcycle lengths outputted from SVR.
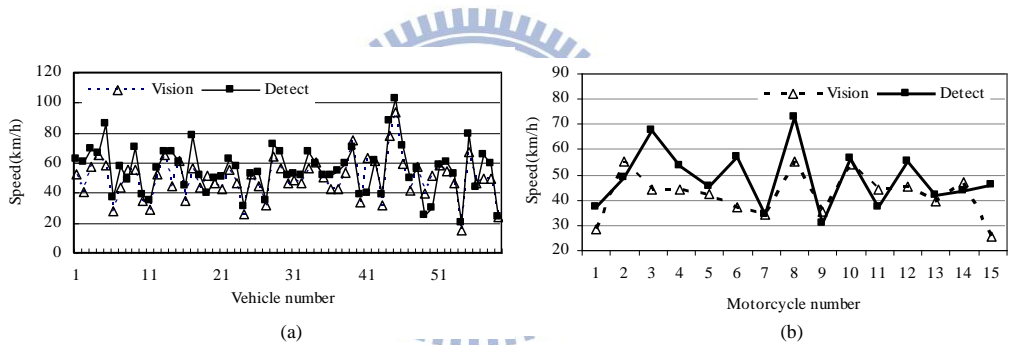

(a)   (b)

Figure 4.4. Estimated vehicle speeds. The open triangles with dashed line are the speeds measured from the video system. The rectangles with black line are the speeds estimated using the proposed algorithm. (a) Estimated speeds for all vehicle categories. (b)Estimated speeds for motorcycles.

Table 4.7.   Virtual loop length for each lane.

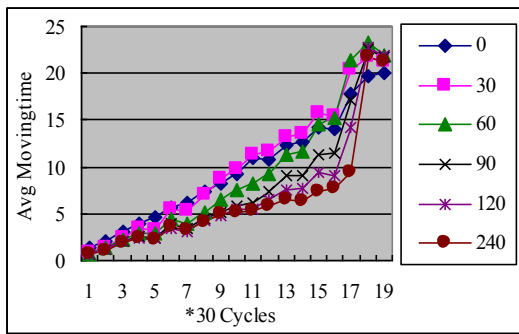|	Lane1	Lane2	Lane3	Lane4
Virtual loop length	7.9 m	8. 1m	9.2 m	9.9 m

4.2 Three new traffic parameters

The test example in Table 4.8 involves two adjacent intersections with a 700 foot link at a fixed-timed traffic signal operating with 60-s cycle length and 23-s effective green interval. To determine the features of the three parameters and the effects of environmental change, eight scenarios were prepared and listed in Table 4.8: traffic flow changing from 48 vph to 2880 vph, different detector zone size (20, 50 feet), different vehicle detector distances to the stop bar (0, 30, 60,90,120,240 feet), and next intersection spill back. Figure 4.5 shows the results of one scenario involving changing flows and vehicle detector distances from the stop bar. Each point of each sub-graph is the average of 30 continued cycles which share the same traffic flow. Sub-graphs (a), (c) and (e) show the normal flow. Sub-graphs (b), (d) and (f) show the spill-back flow. Notably, Moving time is directly proportional to traffic flow before the occurrence of traffic jams. Additionally, the Stopped time changes slowly when the vehicle detector is not far from the stop bar. Interestingly, the near vehicle detector has a smooth trend for each traffic parameter and the traffic parameters of the far vehicle always jump to some value. If the next intersection is spill-back, the Stopped time is greater than the red phase time and the Moving time is less than the green phase time. Table 4.8 lists the summarized relationships between three traffic parameters and the environment. The arrows in Table 4.8 denote the trend of traffic parameters.

The other test example for arrival shockwave involves two adjacent intersections with a 997 foot link at a fixed-timed traffic signal operating with a 60-s cycle length and a 30-s effective green interval. Two electronic vehicle detectors are located 300 and 570 feet from the stop bar. The change sequence for the traffic flow is 650, 550, 600,
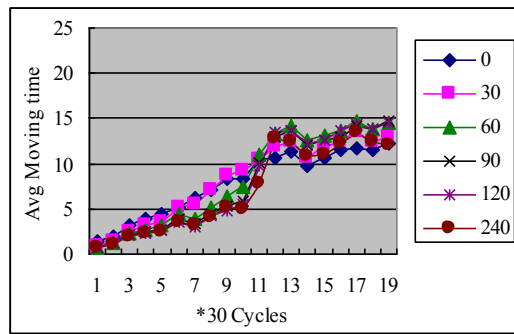
500, 700, 550, 400, 600 and 1000vph every 900 seconds. Since the capacity is 600 vph, the v/c values vibrate around 1 and traffic queues are formed. The sub-graph (a) and (b) of Figure 4.6 display three traffic parameters in two electronic vehicle detectors. Notably, the Stopped time of VD2 is always zero, indicating no traffic queue over VD2. Furthermore, the Stopped time of VD1 occasionally approaches the effective red time (30). Restated, VD1 shows some traffic queues. The sub-graph (a) and (b) of Figure 4.6 illustrate △Stopped time and Moving/(Moving+Empty) of VD1 and VD2.

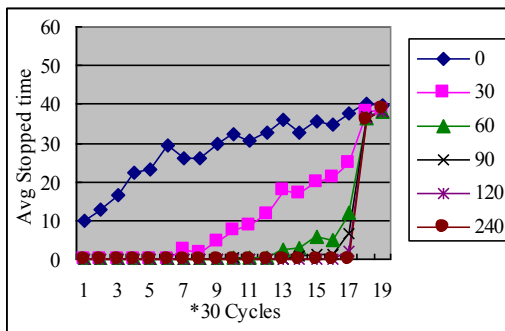Table 4.8.   Summarized relationships between three traffic parameters and the environment.

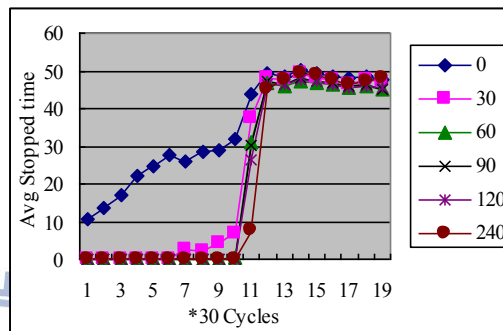| Flow				Empty	Stopped	Moving
	2880 ↗ 48		20 feet	6	38	16
			50 feet	0	38	22
			VD to stop bar	far / near	near / far	near / far
			Spill-back	no / yes	no / yes	no / yes
	2880 ↘ 48		20 feet	6	38	16
			50 feet	0	38	22
			VD to stop bar	far / near	far / near	far / near
			Spill-back	no / yes	no / yes	no / yes

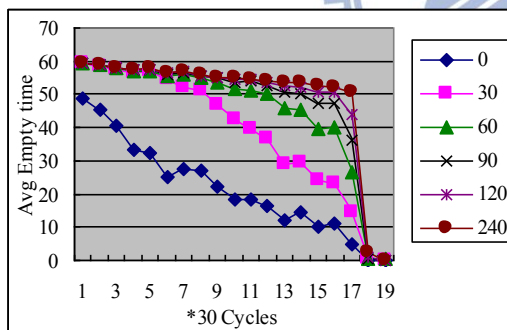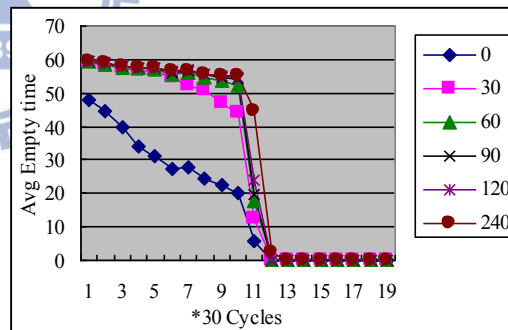(a)

(b)

(c)

(d)

(e)

(f)

Figure. 4.5. Relationships between the three traffic parameters and VD distance from the stop bar (a) Average Moving time for normal traffic flow.   (b) Average Moving time for spill-back. (c) Average Stopped time for normal traffic flow. (d) Average Stopped time for spill-back. (e) Average Empty time for normal traffic flow. (f) Average Empty time for spill-back.
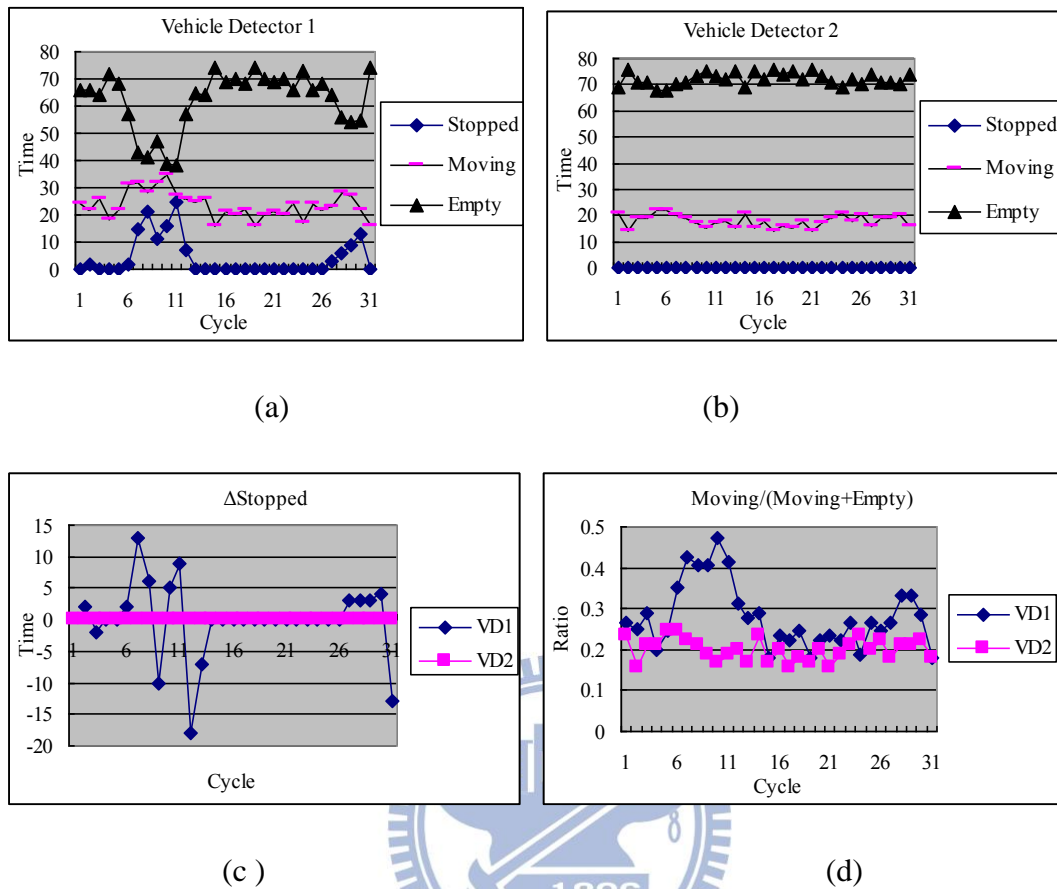
(a)   (b)

(c)   (d)

Figure 4.6. (a)Stopped, Moving and Empty durations in VD1. (b) Stopped, Moving and Empty durations in VD2. (c) △Stopped duration in VD1 and VD2. (d) Moving/(Moving+Empty) in VD1 and VD2

4.3 Shockwave detection

A CORSIM simulation environment has been established to evaluate the traffic parameters and the proposed shockwave detection methods. An independent intersection with four approaches is created in the CORSIM environment. Two vehicle sensors are located 300 and 730 feet from the stop line on an approach from off-ramp, as Figure 4.7 shows. Figure 4.8 illustrates the phase time and input traffic flow of that approach. To demonstrate the capability of the proposed method, the traffic signal

78

timing in this simulation is designed to be dynamically changed. The change of phase time may be resulting from some adaptive control methods; as the traffic flow increases, the green time also increases.
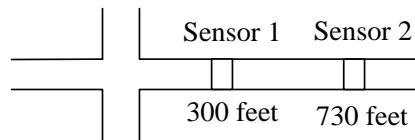

Fig. 4.7. The intersection of simulation: a link and two sensors' locations

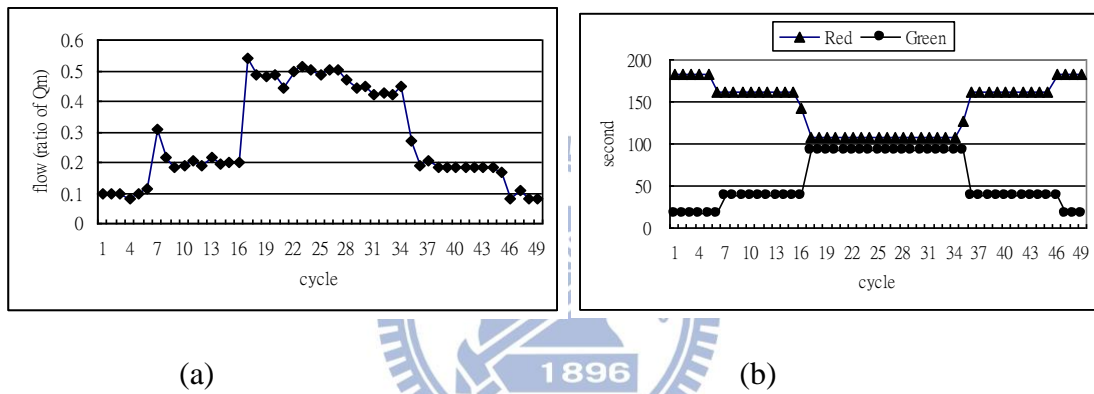(a)   (b)

Figure 4.8 (a) the phase times of the intersection. (b) The input flow of the link.

Figure 4.9 shows the traffic parameters derived from both vehicle detectors during the simulation period. Due to changes in phase duration, some cycle length is shorter or longer than others are. With low traffic flow demands, both detectors output empty duration and moving duration. The stopped duration is only presented when traffic queue reaches the detecting zone. Figure 4.10 compares the red phase duration and the stopped duration of both detectors. Notably, the stopped duration of both detectors approaches the red time, indicating that queue length of un-discharged vehicles reaches beyond the second detector. Moreover, since the first detector is installed closer to stop line than the second one, the first detector would always have more cycles that reports stopped duration.

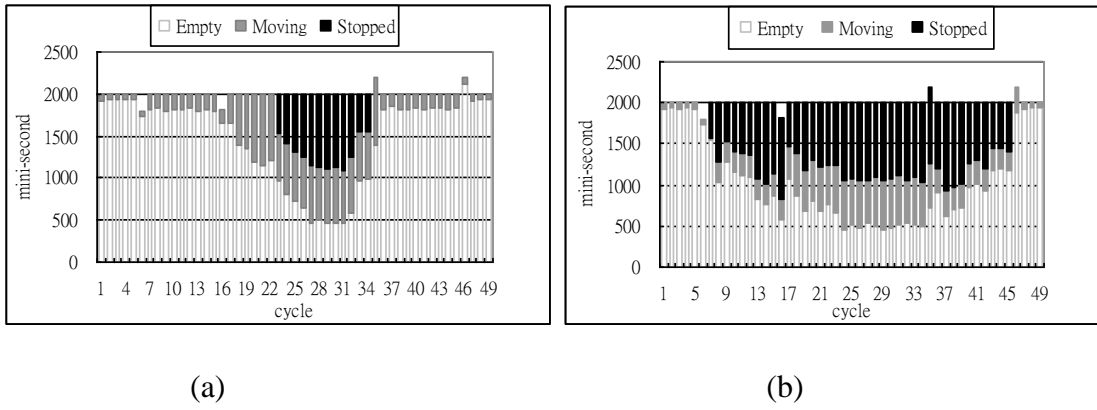(a)   (b)

Figure 4.9 (a) The stopped duration, moving duration and empty duration of detector 1.

(b) The stopped duration, moving duration and empty duration of detector 2.
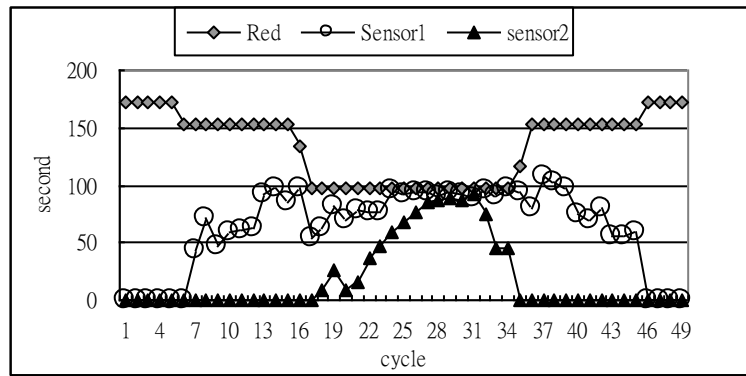
Figure 4.10   Relation between the stopped duration and red phase time.

Results of shockwaves

According to previous discussed shockwave concept, each method of the backward

forming shockwave is valid only for a specific circumstance. For example, Eq. (3.18)

should be used when no stopped duration occurs, otherwise Eq. (3.29) and (3.30) should

be used instead. If the stopped duration be equal to red phase duration, Eq. (3.31) can be

taken into consideration. The constant a in those equations is calibrated as 2.1. The

algorithm proposed in section 3.3 indicates the proper usage of each equation. Figure

4.11 demonstrates the backward forming shockwave calculation of each method and the

final result of the proposed algorithm. In figure 4.11, $\triangle Si$ represents the   tenth of

80

the stopped duration difference of detector *i* for two consecutive cycles ; while *S-i*, *M/E-i*, and *Mavg* denote the shockwave calculated from stopped duration, moving/empty duration, and moving average, respectively. The calculated backward forming shockwave from the proposed algorithm is denoted as W_{30}. It can be observed in Figure 4.11 that the speed of backward forming shockwave is negatively related to the stopped duration difference. As the stopped duration difference decrease, the backward forming shockwave speed increase, vice versa. The condition should holds theoretically. However, with stochastic driving behavior, some non-ordinary driving behavior occurs near the vehicle detector on the 17th cycle of simulation. Therefore, the statement would be violated on the 17th cycle.
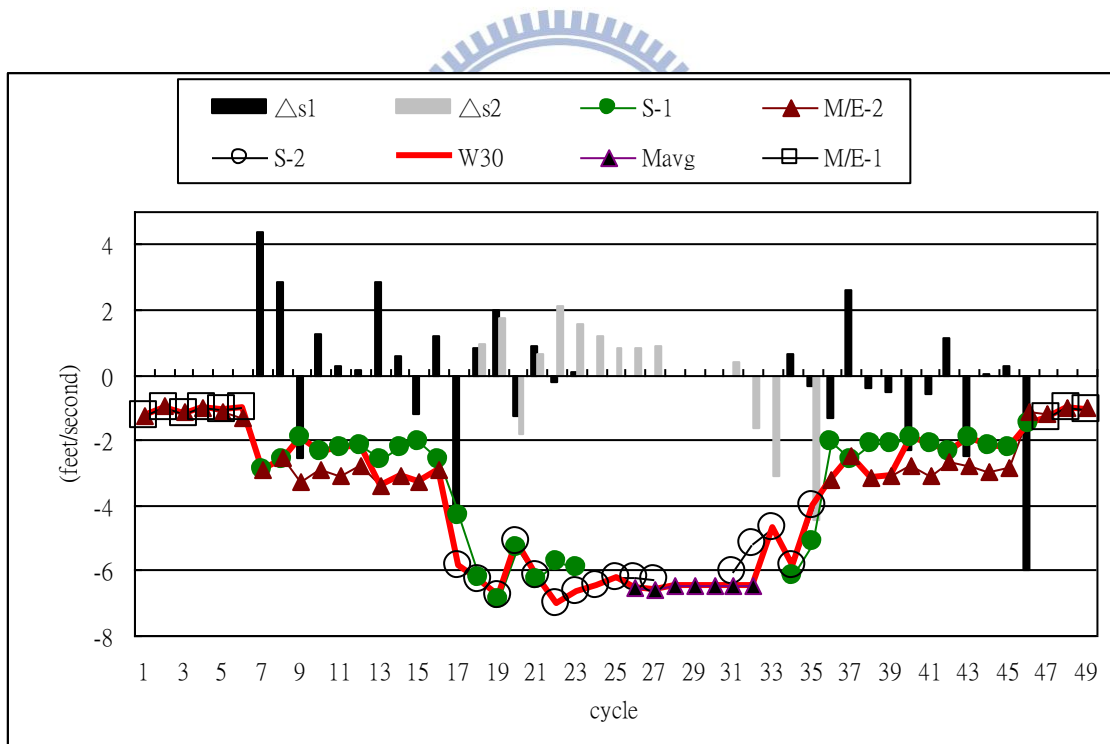

Figure 4.11 Results of the backward forming shockwave detection algorithm.

Figure 4.12 compares the shockwave calculating result derived from detector with the one that directly measured from CORSIM. In Figure 4.12, the ideal forward

recovery / backward forming shockwave is denoted as W_{21} / W_{20}; while W_{31} / W_{30} denotes the calculated forward recovery/ backward forming shockwave. The directly measured ones are denoted as W^*_{31} and W^*_{30}, respectively. In Figure 4.12, the calculated shockwaves are similar to the directly measured ones, which represent a significant result. In the simulation, the intersection has a fixed saturation flow rate, without the disturbance from downstream spillover; therefore, W_{01} would maintain a stable value (-21 ft/sec herein).
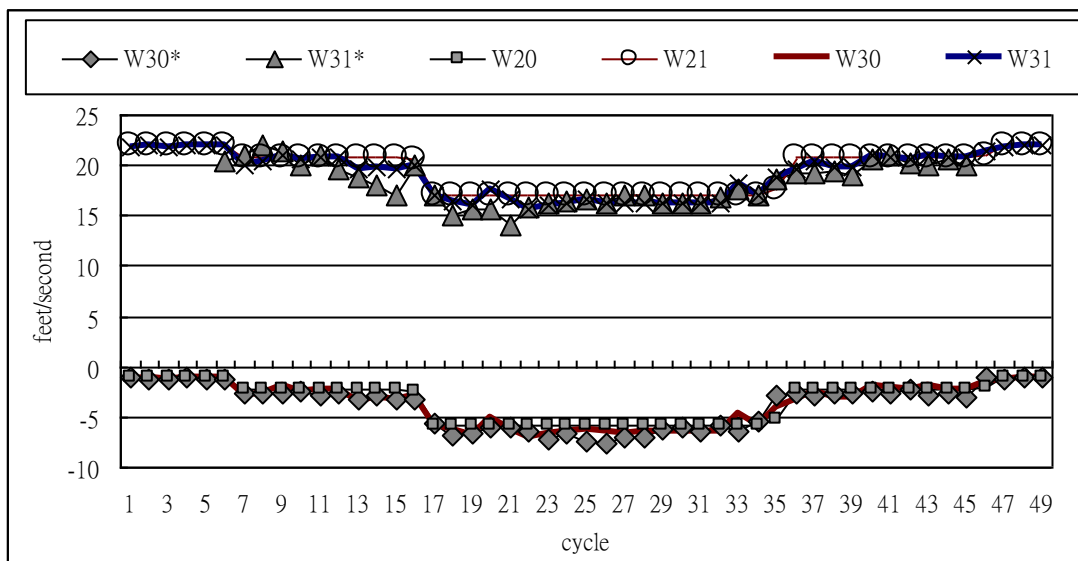
Figure 4.12 Comparison of calculated / directly-measured shockwaves of the approach.

The mean absolute percentage error (MAPE) of W_{30} is 12.4% and the mean absolute error (MAE) is 0.42 ft/sec. While the MAPE and MAE of W_{31} is 4% and 0.69 ft/sec respectively. The bias mainly comes from the vehicle arrival pattern; as the vehicle comes uniformly as Figure 4.13(a), the detected stopped duration and corresponding shockwave detection would be unbiased. If vehicles arrive as platoons as shown in Figure 4.13 (b) or (c), the inaccurate stopped duration would result biased W_{30}. Figure 4.13(b) demonstrates that, as the queue results from the first platoon does not

reach detector and there exists a major gap between the first and the second platoon, the stopped duration would be underestimated. The underestimated stopped duration would result in a slower shockwave speed (indicated as dash line). Figure 4.13(c) gives the counter example of overestimated stopped duration and the corresponding faster shockwave speed. During the simulation, it is observed that with more congested traffic; the less probability of major gap would happen.
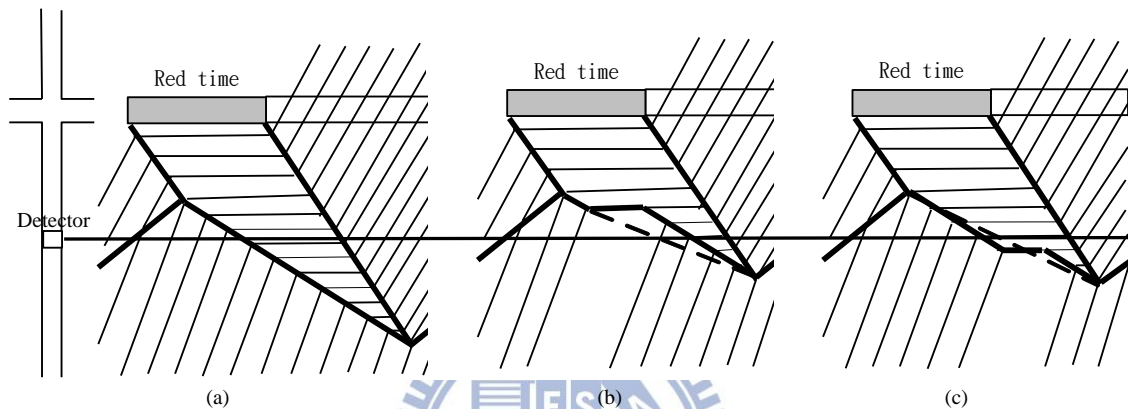
Figure 4.13. The comparison of different arrival pattern and its corresponding bias in shockwave estimation. (a) Uniform arrival pattern and its corresponding shockwave, (b) arrival pattern that gives an underestimated shockwave speed, and (c) arrival pattern that gives an overestimated shockwave speed.

4.4 Upstream flow and speed detection

In Figure 4.14, the estimated upstream flow is compared with the simulation input. To give a better understanding, these flow rates have been transformed into flow ratio (r). The flow ratio (r) is then compared with the flow ratio derived from simulation ($r*$). The comparison of estimated upstream speed (U) and detected speed (U*) is illustrated in Figure 4.15. The estimated upstream speed (U) is space mean speed but the detected speed is time mean speed; therefore, the detected speed is transformed to space mean

speed with the method proposed by Drake, Schofer, and May [47]. The MAPE and MAE of flow ration are 18% and 0.03 respectively. While those of space mean speed are 4% and 1.79ft/sec respectively. These results demonstrate that the proposed algorithm is capable of estimating flow and speed at upstream area.

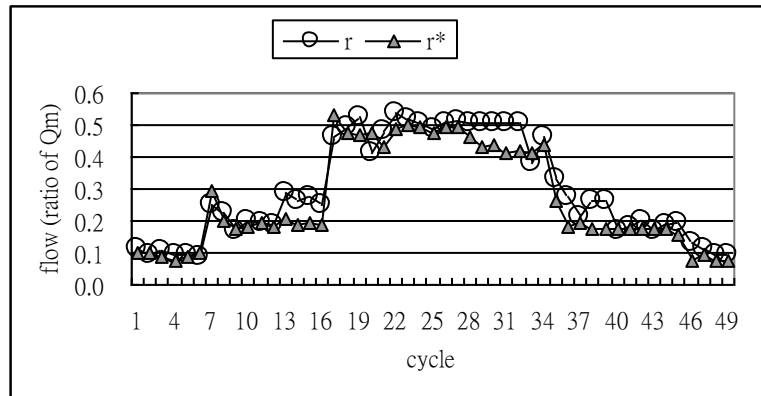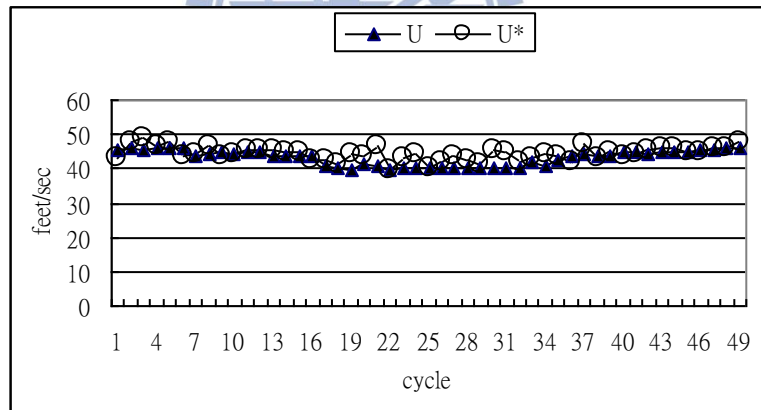Figure 4.14.The predicted traffic flow of state 3

Figure 4.15 The predicted traffic speed of state 3

4.5 Traffic signal control algorithm

To investigate the performance, the proposed model will adjust the maximal green time dynamically according to flow demands. The enhanced actuated control will be compared with traditional full-actuated control which's maximal green time is fixed generally.

This study employs a closely spaced intersections consisting of three intersections. Basic layouts and phase configurations are given in Figure 3.16 and Figure 3.17(b). The spacing between intersections is set to be 200 feet. The numerical test includes 10 demand entries (A-J) and two volume levels (stable and unstable) designed to test the performance of proposed control model. Table 4.9 summarizes all experimental scenarios. The stable demand entries in all critical paths have the same volume. The unstable demand scenario has different peak periods for four critical paths.

Table 4.9. Experimental scenarios for model evaluation

Demand scenario	Path	Demand entries (in vph)									
		A	B	C	D	E	F	G	H	I	J
Stable	1	700	700	700	700	700	700	700	700	700	700
	2	700	700	700	700	700	700	700	700	700	700
	3	700	700	700	700	700	700	700	700	700	700
	4	700	700	700	700	700	700	700	700	700	700
Unstable	1	700	800	900	900	800	700	600	600	600	600
	2	600	600	600	600	600	600	700	800	900	900
	3	600	600	600	600	700	800	900	900	800	700
	4	900	900	800	700	600	600	600	600	600	600

The proposed model was coded in C++ and tested under the runtime extension of CORSIM. The CORSIM is used as an evaluator. To overcome the stochastic nature of a microscopic simulation system, an average of 10 simulation runs has been used. For the measure of effectiveness (MOE) comparison, since CORSIM calculates total delays or average delays only for departed vehicles, it is not computationally convenient to use delay as the MOE for over-saturated conditions. Hence, in this study we use total queue time, maximal queue, queue delay and speed as the MOE.

The overall results of proposed model and full-actuated method under different traffic demands (as indicated in Table 4.9) are compared in Table 4.10. Compared to ordinary full-actuated scheme, this proposed methodology would improve the total queue time of 13.8% under stable demand situation; while under unstable demand, this value would increase to 31%. Other performance indexes are laid out in Table 4.10. It is clear that compare to ordinary full-actuated scheme, the proposed model works even better in the unstable-demand scenario. This improvement can be creditable to the path-based progression and the dynamic maximal green times among critical paths.

Table 4.10 Comparison of CORSIM simulation results.

Scenarios	MOEs	Simulation results from CORSIM (4h)		
		Proposed	Full-act	Improvement[a](%
Stable–demand	Total queue	8476.7	9829.4	13.8
	Maximal queue(veh)	12.6	13.4	6.0
	Queue delay(sec/veh)	45.4	52.7	13.8
	Speed(MPH)	6.5	5.8	12.0
Unstable-demand	Total queue	9257.6	13407.8	31.0
	Maximal queue(veh)	19.9	33.8	41.1
	Queue delay(sec/veh)	49.4	71.2	30.6
	Speed(MPH)	9.3	7.3	27.6

[a] Improvement is calculated by $(MOE_{proposed} - MOE_{actuacted})/MOE_{actuated}$

Figure 4.16 demonstrates the dynamic change of maximal green time according to its corresponding demand on different critical paths. To evaluate the performance of the proposed method, this study compares indexes on critical paths i.e., the queue time, queue delay and speed for each path under different demand scenarios. The comparison of indexes is demonstrated in Figure 4.17 through Figure 4.19. The proposed model outperforms the ordinary full-actuated control scheme among all paths. Under both stable and unstable demand scenarios (see Figure 4.17 and 4.18), the proposed model can deliver a more efficient control strategy than ordinary full-actuated control scheme.

With the proposed model, all paths have improved queue time, maximal queue, queue delay, and speed compared to ordinary full-actuated method.
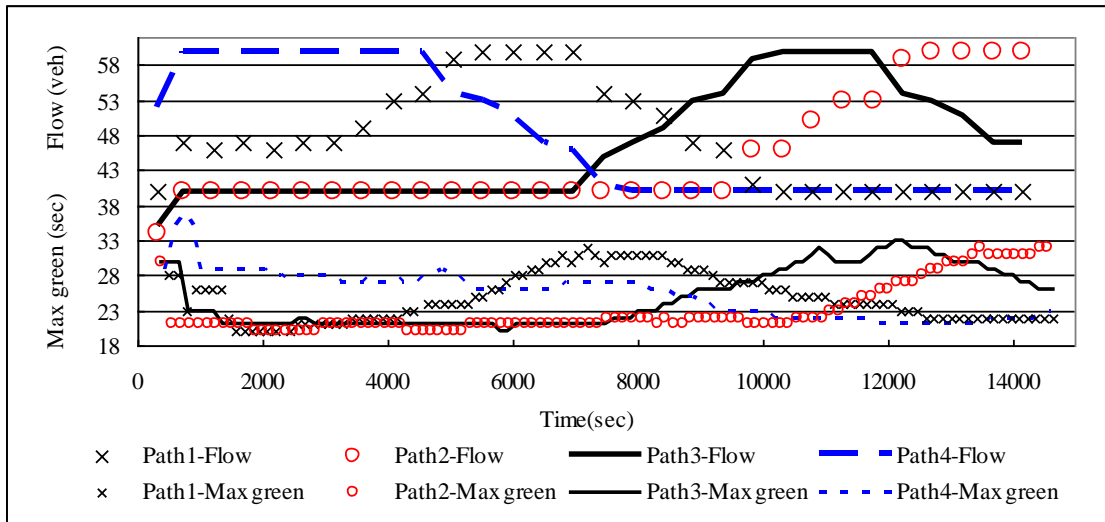

Figure 4.16　Relation between the maximal green time and traffic flow for proposed model.
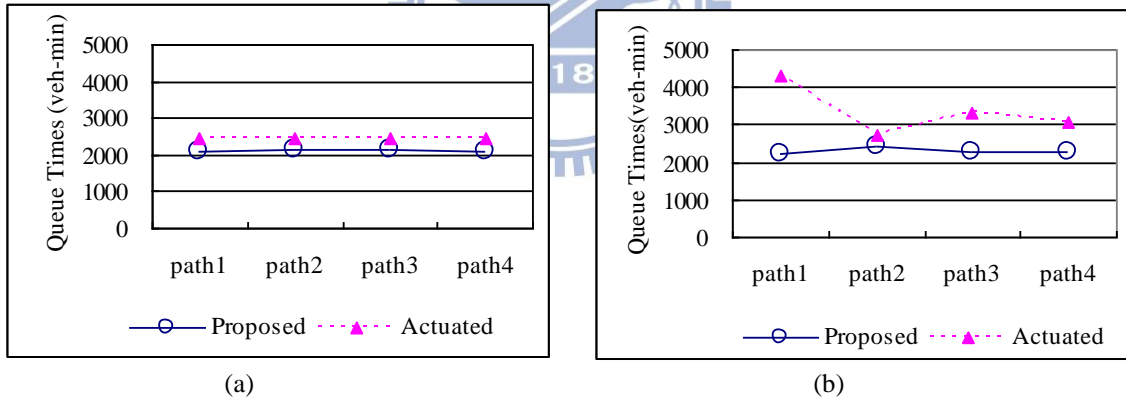

(a)   (b)

Figure 4.17 Queue times of paths under (a) stable demand (b) unstable demand.
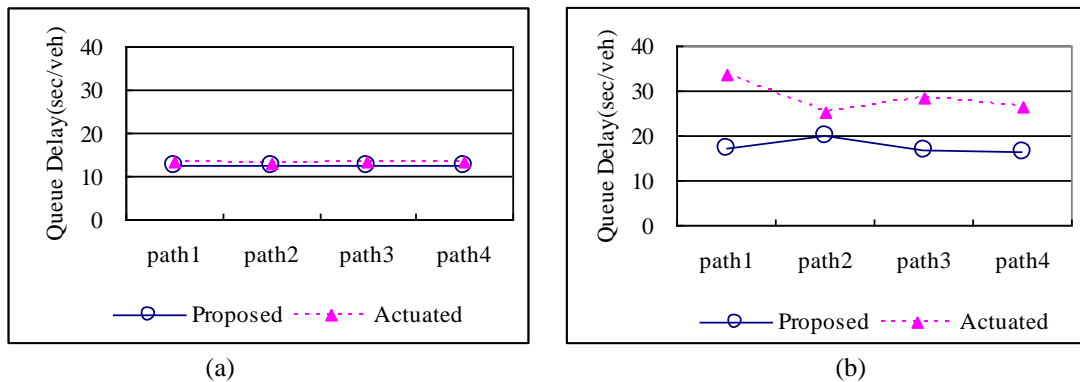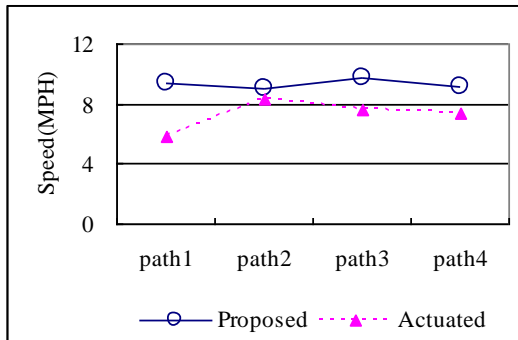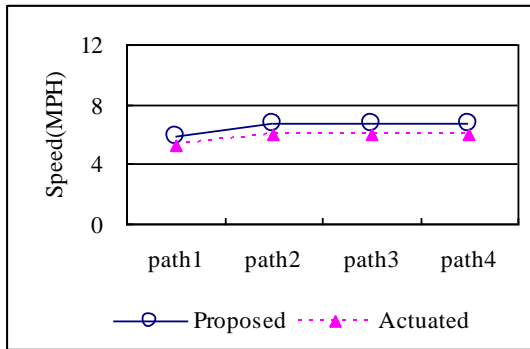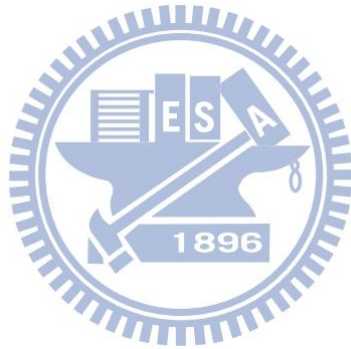

(a)   (b)

Figure 4.18 Queue delay of paths under (a) stable demand (b) unstable demand.

Figure 4.19 Speed of paths under (a) stable demand (b) unstable demand.

V. Conclusions

In this study, a CMOS based transceiver with STC antenna has been successfully implemented for advanced traffic signal processing. The collected radar signals from the CMOS radar system have been processed with developed optimization algorithms for vehicle-type classification and speed determination. The high recognition rate optimization algorithms are mainly based upon the information of short setup time and different environmental installation of each sensor. The algorithm includes four phases, namely signal processing, calibration, learning and 'classification and speed estimation'. In the calibration and learning phases, a video recognition module has been further adopted as a supervisor of SVM and SVR. SVM has successfully classified vehicles into four categories: motorcycles, small, medium and large vehicle in the classification phase. SVR has estimated vehicle lengths and determined their speeds accurately in the speed estimation phase. Specially, the proposed algorithm can detect motorcycles and estimate their speeds precisely. Compared with conventional circuit-based detector systems, the developed CMOS radar integrates submicron semiconductor devices and thus not only possesses low stand-by power but also is ready for production. In the meanwhile, the algorithm has successfully provided a high recognition rate in a grey area which traditional unsupervised classifiers have low recognition rates and supervised classifiers are hard to prepare training data. Furthermore, the developed algorithm of this study simultaneously optimizes the vehicle-type classification and speed determination in a computationally cost-effective manner, which benefits real-time intelligent transportation system. In the future, the enhanced vehicle length and speed accuracy can be obtained by applying SVR to each category of vehicles.

Another direction for future research could be to apply the SVM model to vehicle signals of each lane.

In this study, we also proposed an innovative approach to estimate the upstream traffic information at intersection under oversaturated situation using shockwave analysis. A key methodological contribution of the approach is that it estimates shockwaves by combining traffic parameters, dynamic traffic signal timing and traffic flow models. By utilizing parameters of stopped duration, moving duration, and empty duration, that are estimated form the presence of the radar detector, we are able to calculate shockwaves including 1) forward recovery, 2) ideal backward forming, 3) ideal forward recovery, 4) backward forming, and 5) forward recovery shockwave.

To the best of authors' knowledge, this is the first study that utilizes real time shockwave by stopped duration to estimate upstream traffic flow and speed far beyond detection zones of vehicle detectors. With the shockwaves, upstream traffic flow and speed information can be estimated accordingly. These models are evaluated by traffic simulation and demonstrate a significant result. The proposed model has some pre-conditions for traffic flow state. These assumptions can be solved by combining linear regression and the information derived from multi-zone sensors to capture the variation of shockwaves.

Traditional full-actuated control scheme would work well only on an intersection or arterials. In closely spaced intersections, it might suffer from capacity loss, poor coordination and long congestion time due to considering only gap-out criterion, non-path-based progression and fixed maximal green time, respectively. With the above, a novel actuated critical path control model for designing traffic signal timings in closely spaced intersections had been presented.

A network had been exemplified with micro-simulation to illustrate the

effectiveness of the proposed method. The numerical example demonstrates a satisfying result compare to ordinary full-actuated scheme. Compared to ordinary full-actuated scheme, under stable demand this novel methodology would improve the total queue time, maximal queue, queue delay, and speed of 13.8%, 6%, 13.8%, and 12%, respectively; while under unstable demand, these values would increase to 31%, 41.1%, 30.6%, and 27.6%.

This study has several key contributions, including 1) developing a radar vehicle detection algorithm to simultaneously optimize the vehicle-type classification and speed determination, 2) using the presence of radar sensor to compute the stopped, moving and empty durations; and combining them to estimate the shockwaves, 3) introducing shockwave detection theory to dynamically adjust maximal green time for critical path with unstable traffic demands, 4) designing a path-based progression scheme that suitable for closely spaced intersections, 5) providing a traffic signal control method which can use fewer detectors than traditional traffic signal control scheme.

Reference

[1]   A. Stove, "Linear FMCW Radar technigues," in *IEE Proceedings-F*, 1992, pp. 343–350.

[2]   D. E. Barrick, "FMCW Radar signals and digital processing," National Oceanic and Atmospheric Administration, Tech. Rep., 1973.

[3]   D. V. Arnold, J. B. D. JR., and B. C. Files, "Systems and methods for monitoring speed," in *US Paten No. 7426450 B2*, 2008.

[4]   H. H. W.-H Lin, J. Dahlgren, "An enhancement to speed estimation using single loop detectors," in *Proceeding of Intelligent Transportation Systems*, 2003.

[5]   J. J. Reijmers, "On-line vehicle classification," *IEEE Transactions on Vehicular Technology*, vol. 29, pp. 156–161, 1980.

[6]   H.-S. Lai and H.-C. Yung, "Vehicle-type identification through automated virtual loop assignment and block-based direction-biased motion estimation," *IEEE Transaction on Intelligent Transportation Systems*, vol. 1, pp. 86–97, 2000.

[7]   H. Roe and G. Hobson, "Improved discrimination of microwave vehicle profiles," *Microwave Symposium Digest, IEEE MTT-S International*, vol. 2, pp. 717–720, 1992.

[8]   S. J. Park, T. Y. Kim, S. M. Kang, and K. H. Koo, "A novel signal processing technique for vehicle detection Radar," *Microwave Symposium Digest, IEEE MTT-S International*, vol. 1, pp. 607–610, 2003.

[9]   P.-F. Pai, "System reliability forecasting by support vector machines with genetic algorithms," *Mathematical and Computer Modelling*, vol. 43, pp. 262–274., 2006.

[10] Q. He, Z.-Z. Shi, and L.-A. Ren, "A novel classification method based on hypersurface," *Mathematical and Computer Modelling*, vol. 38, pp. 395–407, 2003.

[11] L. Edler, J. Grassmann, and S. Suhai, "Role and results of statistical methods in protein fold class prediction," *Mathematical and Computer Modelling*, vol. 33, pp. 1401–1417, 2001.

[12] J. Duchene and S. Leclercq, "An optimal transformation for discriminant and principal component analysis," *IEEE Transactions on PAMI*, vol. 10, pp. 978–983, 1988.

[13] R. A. Fisher, "The use of multiple measures in taxonomic problems," *Ann. Eugenics*, vol. 7, pp. 179–188, 1936.

[14] M. J. Lighthill and G. B. Whitham., "On kinematic waves: a theory of traffic flow on long crowded roads," *Proceedings of the Royal Society of London*, vol. 229A, pp. 317–345, 1955.

[15] P. G. Michalopoulos, "Shock waves in traffic signal analysis and control," in *American Control Conference*, 1982.

[16] A. D. May, *Traffic Flow Fundamentals*. Prentice Hall, 1990.

[17] H. X. Liu, X. Wu, W. Ma, and H. Hu, "Real-time queue length estimation for congested signalized intersections," *Transportation Research Part C-Emerging Technologies*, vol. 17, pp. 412–427, 2009.

[18] D. C. Gazis, "The origins of traffic theory," *Operations Research*, vol. 50, pp. 69–77, 2002.

[19] D. C. Gazis, *Traffic Science*. John Wiley Inc., 1974.

[20] D. L. Gerlough and M. J. Huber, *Traffic flow theory: a monograph*. Transportation Research Board, 1975.

[21] T. Kim and H. Zhang, "A stochastic wave propagation model," *Transportation Research Part B-Methodological*, vol. 42, pp. 619–634, 2008.

[22] H. M. Zhang, "A theory of nonequilibrium traffic flow," *Transportation Research*

Part B-Methodological, vol. 32, pp. 485–498, 1998.

[23] G. Abu-Lebdeh and R. F. Benekohal, "Development of traffic control and queue management procedures for oversaturated arterials," *Transportation Research Record*, vol. 1603, pp. 119–127, 1997.

[24] H.-J. Cho and M.-T. Tseng, "A novel computational algorithm for traffic control soc," *WSEAS Transactions on Mathematics*, vol. 5, pp. 123–128, 2006.

[25] F. Diona, H. Rakhab, and Y.-S. Kangc, "Comparison of delay estimates at under-saturated and over-saturated pre-timed signalized intersections," *Transportation Research Part B-Methodological*, vol. 38, pp. 99–122, 2004.

[26]H.-J. Cho and S.-C. Lo, "Modeling self-consistent multi-class dynamic traffic flow," *Physica A*, vol. 312, pp. 342–362, 2002.

[27] H.-J. Cho and Y.-T. Wu, "Microscopic analysis of desired-speed car-following stability," *Applied Mathematics and Computation*, vol. 196, pp. 638–645, 2008.

[28] B. D. Greenshields, "A study of traffic capacity," *Proceedings of the Highway Research Board*, vol. 14, pp. 448–477, 1934.

[29] P. G. Michalopoulos, G. Stephanopoulos, and G. Stephanopoulos, "An application of shock wave theory to traffic signal control," *Transportation Research Part B-Methodological*, vol. 15, pp. 35–51, 1981.

[30] X. Wu, H. X. Liu, and D. Gettman, "Identification of oversaturated intersections using high-resolution traffic signal data," *Transportation Research Part C-Emerging Technologies*, vol. 18, pp. 626–638, 2010.

[31] A. Skabardonis, "Determination of timings in signal systems with traffic-actuated controllers," *Transportation Research Record*, vol. 1554, pp. 18–26, 1996.

[32]F. Webster, "Traffic signal settings, road research laboratory technical paper no. 39," HMSO,London, UK., Tech. Rep., 1958.

[33] R. L. Gordon and W. Tighe, "Traffic control system handbook, report no.fhwa-hop-06-006," Federal Highway Administration, Tech. Rep., 2005.

[34] D. Husch and J. Albeck, *Synchro 5 User Guide*. Trafficware 1009B Solano Avenue Albany, CA 94706, 2001.

[35] *TRANSYT-7F Release 11 Users Guide*. University of Florida, 2012.

[36] J. D. C. Little, "Maximal bandwidth for arterial traffic signals: Theory and interactive computation," *Working Paper WP 970-78, Alfred P. Sloan School of Management*, 1977.

[37] J. D. C. Little, "The synchronization of traffic signals by mixed-integer linear programming," *Operations Research*, vol. 14, pp. 568–594, 1966.

[38] J. D. C. Little, M. D. Kelson, and N. H. Gartner, "Maxband: A program for setting signals on arteries and triangular networks," *Transportation Research Record*, vol. 795, pp. 40–46, 1981.

[39] T. H. Chang and G. Y. Sun, "Modeling and optimization of an oversaturated signalized network," *Transportation Research Part B-Methodological*, vol. 38, pp. 687–707, 2004.

[40] Z. Tian, T. Urbanik, and R. Gibby, "Application of diamond interchange control strategies at closely spaced intersections," *Transportation Research Record*, vol. 2035, pp. 32–39, 2007.

[41] C. J. Messer, "Simulation studies of traffic operations at oversaturated, closely spaced signalized intersections," *Transportation Research Record*, vol. 1646, pp. 115–123, 1998.

[42] Y. Liu and G. L. Chang, "An arterial signal optimization model for intersections experiencing queue spillback and lane blockage," *Transportation Research Part C-Emerging Technologies*, vol. article in press, 2010.

[43] X. Zheng and L. Chu, "Optimization of control parameters for adaptive traffic-actuated signal control," *Journal of Intelligent Transportation Systems*, vol. 14, pp. 95–108, 2010.

[44] E. Conte and M. Lops, "Clutter-map CFAR detection for range-spread targets in non-gaussian clutter," *IEEE Transactions on AES*, vol. 33, pp. 432–442., 1997.

[45] S. Wang, H.-S. Wu, and C.-H. Chang, "Modeling and suppressing substrate coupling of RF CMOS FMCW sensor incorporating synthetic quasi-tem transmission lines," in *IEEE MTT-S International Microwave Symposium*, 2007, pp. 1939–1942.

[46] C.-K. Tzuang, C.-H. Chang, and H.-S. Wu, "An x-band CMOS multifunction-chip FMCW radar," in *IEEE MTT-S International Microwave Symposium*, 2006, pp. 2011–2014.

[47]H.-J. Cho and M.-T. Tseng, "Shockwave detection for electronic vehicle detectors," *Lecture Notes in Computer Science*, vol. 4490, pp. 275–282, 2007.